Zhang *et al. Alzheimer's Research & Therapy* (2025) 17:55
https://doi.org/10.1186/s13195-025-01704-y

Alzheimer's Research & Therapy

RESEARCH Open Access

HCN2 deficiency correlates with memory deficits and hyperexcitability of dCA1 pyramidal neurons in Alzheimer's disease

Xiaoqin Zhang[1*†], Yiping Zhang[2†], Ting Zhang[1], Jing Wang[2], Chang Liu[1], Qing Shang[3], Xiaojie Wei[2], Huaqiang Zhu[4], Haowei Shen[1*] and Binggui Sun[2*]

Abstract

Background Abnormal excitability of hippocampal neurons may lead to dysfunction of neural circuits and then causes cognitive impairments in Alzheimer's disease (AD). However, the underlying mechanisms remain to be fully elucidated.

Methods Electrophysiology was performed to examine the intrinsic excitability of CA1 neurons and the activity of the hyperpolarization-activated cyclic nucleotide-gated ion channels (HCNs) of CA1 neurons in wild type (WT) and hAPP-J20 mice. The activity of CA1 pyramidal neurons (PNs) was modulated with chemogenetics. The activity of HCNs was regulated with nonselective facilitator (cAMP) or inhibitor (ZD7288) of HCNs. Immunohistochemical staining or western blotting were performed to examine the expression of HCN1 and HCN2 in the hippocampus of WT and hAPP-J20 mice, or AD patients and non-AD controls. AAVs were injected to specifically modulate the expression of HCN2 in dorsal CA1 (dCA1) PNs. Cognitive performance of mice was assessed with behavioral tests.

Results dCA1 PNs were more excitable in hAPP-J20 mice, but the excitability of PNs in the ventral CA1 (vCA1) or PV neurons was comparable between WT and hAPP-J20 mice. The activity of the HCNs was reduced in dCA1 PNs of hAPP-J20 mice, and pharmacologically increasing the activity of HCNs attenuated the hyperexcitability of dCA1 PNs in hAPP-J20 mice, suggesting that the reduced activity of HCNs is associated with the hyperexcitability of dCA1 PNs in hAPP-J20 mice. The expression of HCN2 but not HCN1 was reduced in the hippocampus of hAPP-J20 mice, and the expression of HCN2 was also reduced in the hippocampus of AD patients, suggesting that dysregulation of HCN2 is associated with the reduced activity of HCNs in AD. Overexpressing HCN2 rescued the activity of HCNs, attenuated the hyperexcitability of dCA1 PNs and improved memory of hAPP-J20 mice, and knocking down HCN2 impaired the function of HCNs, increased the excitability of dCA1 PNs and led to memory deficits in WT mice.

†Xiaoqin Zhang and Yiping Zhang contributed equally to this work.

*Correspondence:
Xiaoqin Zhang
zhangxiaoqin1@nbu.edu.cn
Haowei Shen
shenhaowei@nbu.edu.cn
Binggui Sun
bsun@zju.edu.cn

Full list of author information is available at the end of the article

Conclusions Our data suggest that dysregulation of HCNs, particularly HCN2, contributes to the abnormal excitability of CA1 PNs in AD mice and probably in AD patients as well, and thus provide new insights into the mechanisms underlying the aberrant activity or excitability of hippocampal neurons in AD.

Keywords Alzheimer's disease, Aβ, HCN2, CA1 pyramidal neurons, Hyperexcitability

Background

Alzheimer's disease (AD) is the most common neurodegenerative disorder characterized by progressive cognitive impairments [1–3]. The featured hallmarks of AD include extracellular deposition of amyloid β (Aβ) and intracellular tau fibrillary tangles [1, 2, 4]. Although the precise roles of Aβ and tau in AD pathogenesis are not clear, the accumulation of both Aβ and tau leads to abnormal neuronal activity which may account for the dysregulation of the neural circuits and the impaired cognitive functions in AD [5–12]. Previous studies have revealed that selective vulnerability of CA1 PNs plays a key role in the onset of cognitive impairment during the early phases of AD, and the hyperactivity of CA1 PNs is an early event in the pathogenesis of AD [5, 13]. While impaired synaptic transmission may contribute to the hyperactivity of CA1 PNs [6, 14–16], several studies indicate that the disturbed intrinsic membrane properties play major roles in the hyperactivity of CA1 PNs in AD [17–19]. However, the factors accounting for the abnormal intrinsic membrane properties of CA1 PNs in AD remain to be elucidated.

Hyperpolarization-activated cyclic nucleotide-gated channels (HCNs) include four members: HCN1-4[20–22]. They are voltage-gated ion channels that conduct a current termed I_h and are activated upon membrane hyperpolarization [20, 21]. The HCN channels are open at rest, permeable to K^+ and Na^+ ions, and their activation gating is facilitated by cAMP [21]. Among the four HCN members, intense expression of HCN1 and HCN2 but not HCN3 and HCN4 could be observed in the hippocampus of rodents and humans [23–25]. Several lines of studies have demonstrated that HCNs are important in maintaining the membrane properties of neurons, generating theta rhythms and regulating memory formation [22], and disrupted HCNs are associated with different types of neurological disorders such as epilepsy and neurodegeneration [22, 26].

Previous studies have indicated that the dysregulation of HCN channels is involved in the pathogenesis of AD [22]. Saito et al. reported that abnormal signaling of HCN channels was a potential link between epileptic seizures and Aβ generation [27]. Musial et al. reported a mixed HCN channelopathy in the CA1 PNs of 3×Tg and 5×FAD mice, but the expression level of HCN1 in enriched CA1 membrane fractions of these AD mice was similar to that of normal control mice [28, 29]. In hAPP-J20 mice, the expression of both HCN1 and HCN2 was not changed in both DG and CA1 areas [30]. In Tg2576 mice, however, the expression of HCN1 was reduced in CA1 lysates [31]. In AD patients, one study reported that the expression of HCN1 was reduced in the temporal lobe [27]. In a meta analysis, among 8 dataset of mass spectrometry (MS)-based proteomics of the temporal lobes, reduction of HCN1 was only observed in 2 of them [32]. A recent study reported, however, that the expression of HCN1 and HCN2 was increased in the hippocampus of patients with AD [33]. Clearly, the results of studies regarding the alteration of the expression of HCNs in brain tissues of AD patients or mouse models are inconsistent. In a rat model of Aβ pathology, Eslamizade et al. reported that the alterations of intrinsic excitability in CA1 PNs was related to the functions of HCN channels [34]. Treatment with lamotrigine, a non-selective modulator of HCN channels, rescued the activity of HCN channels, attenuated the hyperexcitability of CA1 PNs and improved memory in Tg2576 or APP/PS1 mice [31, 35]. However, it is not clear which subtype(s) of HCNs were affected under the Aβ pathology, and which subtype(s) of HCNs account for the alterations of the intrinsic properties of CA1 PNs in AD.

In the present study, we report that the functions of HCN channels are impaired in the dCA1 PNs of hAPP-J20 mice, and the impaired HCNs contribute to the hyperexcitability of dCA1 PNs in hAPP-J20 mice. Specifically, the expression of HCN2 is reduced in the hippocampal CA1 neurons of hAPP-J20 mice and AD patients. Overexpressing HCN2 rescues the activity of HCN channels, ameliorates the hyperexcitability of dCA1 PNs, enhances the CA1 LTP and improves the cognitive functions of hAPP-J20 mice. In addition, knocking down the expression of HCN2 reduces the activity of HCNs in dCA1 PNs, increases the excitability of dCA1 PNs and impairs memory of WT mice. Our data suggest that the dysregulation of HCN2 is one of the factors accounting for the abnormal intrinsic membrane properties of dCA1 PNs in AD mice.

Methods

Animals

hAPP-J20 mice (JAX, 034836) overexpressing human APP (hAPP) with two mutations (Swedish and Indiana mutations) [36] were used as the AD mouse model. hAPP-J20 mice were bred with CaMKIIα-Cre mice (JAX, 005359) or PV-Cre mice (JAX, 008069) to generate double-transgenic mice for electrophysiological recordings in

hippocampal pyramidal neurons or PV neurons, respectively. All mouse lines were maintained on a C57BL/6 background and housed under standard conditions at 22 °C and a 12 h light: dark cycle with free access to food and water. All experiments were conducted in accordance with the National Institutes of Health Guide for the Care and Use of Laboratory Animals, and these were approved by the Animal Care and Use Committees of Ningbo University and Zhejiang University, China.

Preparation of the Aβ oligomers

Oligomeric Aβ1–42 was prepared as described previously [37]. Briefly, synthetic Aβ powder (GL Biochem, Shanghai, China) was dissolved in ice-cold hexafluoroisopropanol (HFIP) (Sigma-Aldrich, USA) and then diluted with ddH_2O (100 μL HFIP solution + 900 μL ddH_2O). HFIP was then volatilized under high-purity N_2 blowing until the total volume of the solution is about 700–750 μL, which made the concentration of the Aβ solution as 60 μM. Next, the Aβ solution was incubated at room temperature with shaking for 24 ~ 48 h to obtain Aβ oligomers. The Aβ oligomers was checked by western blotting with 6E10 (Biogelend, SIG-39320, 1:1000), and the solution of Aβ oligomers was stored at 4 °C until use.

Stereotaxic injection of virus

Mice were anesthetized with sodium pentobarbital (50 mg/kg) and positioned in a stereotaxic apparatus (68030, RWD, China). A heating pad was used to warm the mice during surgery. Viruses were injected using a glass micropipette with a tip diameter of 15–20 μm, through a small skull opening (< 0.5 mm [2]). Viruses including rAAV-Ef1a-DIO-EYFP-WPRE-pA, pAAV-DIO-hM4Di-mCherry-3Flag, rAAV-CaMKIIα-HCN2-P2A-EGFP-WPREs and AAV-mCaMKIIα-EGFP-shRNAmir (mHCN2) were purchased from the BrainVTA (BrainVTA Technology Co., Ltd., China) and stereotaxically injected into the dCA1 (anterior-posterior, -2.06 mm; lateral, ± 1.74 mm; and vertical, -1.3 mm; the bregma served as the reference point) with 1 μl/hemisphere at a perfusion rate of 0.2 μl/min.

Chemogenetic inhibition of dCA1 PNs

For behavioral tests, mice expressing hM4Di in dCA1 PNs were intraperitoneally injected with Clozapine N-oxide (CNO) dissolved in 0.9% saline (2 mg/kg) once daily for 2 weeks. Behavioral tests were performed 24 h after the last injection of CNO. After behavioral tests, brain slices were prepared from those mice and were used for electrophysiological recordings.

Hippocampal slice preparation and electrophysiology

Mice were anesthetized deeply with sodium pentobarbital and then decapitated. Brain slices for electrophysiological recordings were prepared as described previously [38]. Briefly, the brains were quickly removed and placed in ice-cold solution containing (in mM): 75 sucrose, 87 NaCl, 3.0 KCl, 1.5 $CaCl_2$, 1.3 $MgCl_2$, 1.0 NaH_2PO_4, 26 $NaHCO_3$, 20 D-glucose equilibrated with 95% O_2–5% CO_2. Coronal slices (220 μm in thickness) containing the dCA1 (roughly from bregma – 1.46 to -2.30) or vCA1 (roughly from bregma – 2.80 to -3.40) were cut using a vibratome (Leica VT1200S, Leica Microsystems, Germany). Subsequently, slices were incubated in a chamber with artificial CSF (aCSF) (in mM: 124 NaCl, 3.0 KCl, 1.0 NaH_2PO_4, 1.3 $MgCl_2$, 2.0 $CaCl_2$, 26 $NaHCO_3$, and 20 D-glucose, 295–305 mOsm, equilibrated at 32 °C with 95% O_2-5% CO_2) at least 1 h at room temperature (20–22 °C). Following incubation, the slices were transferred to a recording chamber, where the submerged slices were perfused with aCSF (32 °C) saturated with mixed gas at a flow rate of 2 mL per min.

Standard whole-cell recordings were made using Multiclamp 700B amplifier and Digidata 1550B (Molecular Devices, Axon Instruments, CA, USA) for data acquisition. A vertical two-stage puller (PC-10, NARISHIGE) was used to make glass electrodes (3IN thin-wall GL1.5 OD/1.12 ID, TW150-3, WPI) into pipettes with resistance between 1.5 and 2.0 mOhm when filled with internal. For current-clamp recordings, a K-based internal solution was used (in mM: 120 K-gluconate, 10 KCl, 10 HEPES, 0.5 EGTA, 4.0 Mg-ATP, and 0.3 Na-GTP, 5.0 Phosphocreatine-Na_2; pH 7.2–7.4, 270–280 mOsm). Before recording, the series resistance was monitored and canceled using a bridge circuit, and the pipette capacitance was compensated. After forming the whole-cell current-clamp configuration, the recorded cells were given 10 min for stabilization of their resting membrane potentials. A current step protocol (from – 200 to 500-pA, with a 50-pA increment; inter-pulse interval, 15 s) was then carried out. The sag ratio was calculated by dividing the difference between the peak and steady-state hyperpolarization following a -200 pA current injection. This was quantified using a series of hyperpolarizing steps, including – 50 pA, and the sag amplitude was recalculated from – 200 pA to 0 pA [39]. RMP and input resistance were recorded by a 500-ms duration – 100 pA current injection. The rheobase was the minimum current injected that generated action potentials, and the threshold was the membrane potential that valued from the first current injected step. Spontaneous action potentials (sAPs) were induced and recorded in the whole-cell current clamp mode with the modified internal solution containing (in mM): 100 K-gluconate, 20 KCl, 10 HEPES, 4 Mg-ATP, 0.5 Na_2-GTP and 10 Na_2-phosphocreatine [14]. The bias current was carefully calibrated to ensure accurate assessment of neuronal activity. For voltage-clamp recordings, a cesium-based internal fluid was used

(in mM: 110 cesium methylsulfate, 15 CsCl, 4 Mg-ATP, 0.3 Na_2-GTP, 0.5 EGTA, 10 HEPES, 4 QX-314, 5 Phosphocreatine-Na_2; pH 7.2–7.4, 270–280 mOsm). HCN currents were recorded with a series of 3.0-s hyperpolarizing voltage steps from a holding potential of − 45 mV to − 105 mV. Tetrodotoxin (TTX, 1 μM), tetraethylammonium chloride (TEA, 5 mM) and $BaCl_2$ (500 μM) and picrotoxin (100 μM) were added in the aCSF to block sodium currents and potassium currents, respectively [40]. Additionally, we utilized the P/4 protocol to subtract leak currents from the voltage clamp recordings. Series resistance was normally less than 20 MΩ and recordings exceeding 20% change in series resistance were terminated. All holding potentials were corrected for liquid junction potential. Data were low pass filtered at 1 kHz and digitized at a sampling frequency of 10 kHz. All chemicals used in the patch clamp were purchased from Sinopharm Chemical Reagent Co., Ltd., except as noted.

For LTP recording in CA1, the field excitatory postsynaptic potentials (fEPSPs) were recorded with glass electrodes (~ 3 MΩ tip resistance) filled with aCSF and evoked every 20 s with a bipolar tungsten stimulating electrode (FHC). Stimulus strength was adjusted to ~40% of the maximal fEPSP response, after a 20 min stable baseline was established, LTP was induced by theta-burst stimulation (TBS) (four theta bursts were applied at 15 s intervals; each theta-burst consisted of five bursts, at 200 ms intervals, of five 100 Hz pulses). Data were analyzed offline with Clampfit 10.7 software.

ELISA

To measure the cAMP levels in the hippocampus, brain tissues were lysed using RIPA buffer (Beyotime, Shanghai, China), and the supernatants were collected for experiments. The mouse cAMP ELISA kit was used to determine the levels of cAMP according to the manufacturer's instructions (Shanghai Enzyme-linked Biotechnology, Shanghai, China).

Immunostaining and quantification

Mouse tissue

As described previously [38, 41–43], mice were perfused transcardially with 0.9% saline and brains were removed immediately and immersed into 4% PFA solution. Coronal Sect. (30 μm in thickness, one in tenth series) were prepared with a sliding microtome (Leica) after the brains were saturated in 30% sucrose in PBS.

For immunofluorescence staining, free-floating sections were first blocked with blocking buffer (10% serum, 1% nonfat milk, 0.2% gelatin in PBS containing 0.5% Triton X-100) and were then incubated with the following primary antibodies: mouse anti-GFAP (G3893, Sigma, 1:2000), rabbit anti-Iba1 (019-19741, Wako, 1:300) and 3D6 (Janssen Research & Development, 1:1000), followed by incubation with appropriate secondary antibodies conjugated with 488 (ab150077, Abcam, 1:500) or 594 (ab150116, Abcam, 1:500).

For immunohistochemical staining, after quenching endogenous peroxidase activity by incubation with 3% H_2O_2 in methanol, sections were incubated with the following primary antibodies: rabbit anti-HCN1 (55222-1-AP; Proteintech, 1:500), rabbit anti-HCN2 (ab313873, abcam, 1:200) and 3D6 (Janssen Research & Development 1:1000). After washing, sections were incubated with biotinylated anti-rabbit (90982, Jackson Lab, 1:250) or anti-mouse IgG (BA9200, Vector, 1:250). Binding of the antibodies was detected using the Elite kit (Vector Laboratories) with diaminobenzidine (Sigma) and H_2O_2 for development.

For quantification of $GFAP^+$ and $Iba1^+$ cells, images of hippocampal slices stained with antibodies against GFAP or Iba1 were obtained with Olympus BX61 microscope equipped with a 10x (NA 1.25) objective. The images were then imported into Fiji (Image J, version 2.0.0). Five images spanning between bregma − 1.46 mm and − 3.16 mm per mouse were selected. The numbers of microglia and astrocytes in the hippocampus were manually counted with Cell Counter plugin, and the number of cells was divided by the total area of the acquired field to represent cell density (cells/mm^2).

The Aβ plaque load was calculated as the percent area of the hippocampus covered by 3D6 immunoreactive material. Three coronal sections were analyzed per mouse, and the average of individual measurements was used to calculate group means.

The expression of HCN1 or HCN2 in the hippocampus of mice was detected as described above. The integrated optical density (IOD) from 3 coronal sections per mouse was determined with the Image J analysis system and averaged in two areas of the SLM and the molecular layer of the DG. Levels of HCN1 and HCN2 were expressed as the ratio of IOD in the SLM and the molecular layer of the DG. Three coronal sections were analyzed per mouse, and the average of individual measurements was used to calculate group means.

Human tissue

Paraffin Sect. (7 μm) of hippocampal tissues from individuals with AD (Braak stages of 4–6) and non-AD controls as described previously [42] were obtained from the National Human Brain Bank for Health and Disease at Zhejiang University. Sections went through xylene and a series of ethanol for dewaxing and underwent antigen retrieval with citrate buffer and formic acid before incubation with 3% H_2O_2 in methanol to quench the endogenous peroxidase activity. After washing with PBS containing 0.1% Triton X-100 and blocked in 10% goat serum, the sections were incubated with rabbit

anti-HCN1 (55222-1-AP; Proteintech, 1:500) and rabbit anti-HCN2 (ab313873, abcam, 1:200) for 48 h at 4℃, followed by goat anti-rabbit biotinylated antibody (90982, Jackson Lab, 1:250) for 2 h at room temperature and then avidin-biotin complex (ABC system, Vector Laboratories) for 1 h at room temperature. Binding of the antibodies was detected using the Elite kit (Vector Laboratories) with diaminobenzidine (Sigma) and H_2O_2 for development, followed by hematoxylin-eosin staining for 1 min to visualize the nuclei of cells.

The expression of HCN2 in the human hippocampus was detected as described above. For quantification of the overall density of HCN2 in CA1 area, the IOD from 1 section each individual was determined with the Image J analysis system and averaged in two areas of the CA1 field and the molecular layer of the DG. The relative overall density of HCN2 in CA1 was expressed as the ratio of IOD in the CA1 field and in the molecular layer of the DG. For quantification of the HCN2 in individual CA1 neurons, the IODs from 18 neurons of the CA1 field per section and the extracellular space around each selected neuron was determined with the Image J analysis system. The relative density of HCN2 in individual CA1 neurons was shown as the ratio of IOD in each neuron and in the extracellular space around this neuron. Five individuals of AD patients or non-AD controls were included for the quantifications of the overall density of HCN2 in the field of CA1 and the density of HCN2 in individual CA1 neurons.

Western blot analysis of HCN1 and HCN2

For analysis of HCN1 and HCN2 in the whole hippocampus of mice, hippocampal tissues were homogenized in ice-cold RIPA buffer (Beyotime, Shanghai, China) with a protease inhibitor cocktail (Beyotime, Shanghai, China), using a glass Teflon homogenizer and incubated on ice for 10 min. Homogenates were centrifuged for 12 min at 12,000 g (4 °C), after which supernatants were collected.

For analysis of HCN1 and HCN2 in the membranous fractions of the hippocampus, a subcellular fractionation method was used to obtain membrane proteins in the hippocampus. Briefly, hippocampal tissue was incubated on ice and homogenized with a Teflon-coated motorized homogenizer. To restore isotonic conditions, 0.32 M sucrose was added at 10 vol of the 10 mM HEPES (pH7.4, containing protease inhibitors cocktail). Then, the samples were centrifuged at 900 g at 4 °C for at least 10 min to remove nuclei and debris and the supernatant containing the membrane, organelles, and cytosolic fractions was collected. The supernatant was further centrifuged (10,000 g) at 4 °C for 20 min. The pellet was collected and centrifuged (20,000 g) at 4 °C for 20 min for two times. The supernatant containing the cytosolic fraction was removed from the pellet containing the enriched membrane fraction. The membrane fraction was then resuspended in a 1% SDS in PIPA solution.

The protein concentrations of the whole hippocampal lysates and the membrane fraction lysates were determined by the BCA assay. Proteins were separated by electrophoresis and then transferred to a nitrocellulose membrane (BioRad, Hercules, California, USA). The membrane was blocked in 5% milk-TBST at RT and probed with rabbit anti-HCN1 (55222-1-AP, Proteintech, 1:2000), rabbit anti-HCN2 (55245-1-AP, Proteintech, 1:1000), mouse anti-GAPDH (sc-137179, Santa Cruz, 1:10000), and anti-caveolin-1 (66067-1-AP, Proteintech, 1:10000) at 4 °C overnight and then reacted with goat anti-rabbit HRP antibody (SA00001-2, Proteintech, 1:5000) or goat anti-mouse HRP antibody (SA00001-1, Proteintech, 1:5000) for 120 min. Detection and quantification of specific bands were performed using a fluorescence scanner (Odyssey Infrared Imaging System, LI-COR Biotechnology, Lincoln, NE, USA). GAPDH and caveolin-1served as the loading controls for whole hippocampal lysates and lysates of membrane fractions, respectively.

Behavioral tests

All behavioral experiments were performed between the ages of four to six months. Intervals between each behavioral test were 1–3 days, which was to ensure sufficient rest for mice. The apparatus was thoroughly cleaned with 70% ethanol between the tests. The behavioral data were recorded and analyzed by ANY-maze software (Stoelting, UK). All tests were performed and analyzed by experimenters who were blind to the genotypes of animals and drug treatments.

Y-maze

The Y maze test was used to assess the spatial working memory (via spontaneous alternations) and exploratory activity (via total number of arm choices). The device was a three-arm horizontal maze (40 cm long and 10 cm wide with 25 cm high) in which the angle between each of the two adjacent arm is 120°. Mice were placed at the center of the three arms and allowed to explore freely for 8 min. The total arm entries and sequences of each arm were recorded. The percent alternations were defined as the proportion of arm choices that differed from the last two choices.

Novel location recognition (NLR)

Mice were first habituated to the open field box for three days, 10 min a day. During training, 24 h after the last habituation, mice were allowed to explore two identical objects for 10 min, two hours later, one of the objects was picked up and placed diagonally opposite the other and mice were allowed again to explore two objects for 5 min.

The time of investigation for each object was measured. The investigation time was measured for each case in which a mouse's nose touched the object or was oriented toward the object and came within 2 cm of it. The discrimination index was defined as (novel location investigation time - familiar location investigation time) / (novel location investigation time + familiar location investigation time).

Three chamber tests

Three chamber tests were performed as described previously to detect rodent sociability and social novelty. The apparatus was consisted of a three-compartment white Plexiglas box (20 cm × 40 cm × 20 cm), a central chamber and two side champers. In the middle of dividing walls, there were rectangular opening (6 cm × 8 cm, equipped with sliding doors) to allow mice moving freely between chambers. Two identical inverted wire cups were placed separately in the corner of each side chamber, whose walls have long vertical openings that are large enough to allow mice outside the cylinder to easily contact the mice inside by sight, hearing and smell. During the habituation phase, the test mice were placed in the middle chamber and allowed to freely explore for 10 min. In the sociability stage, a stranger mouse (the same age, sex, and strain) was placed in a wire cup on one side, then released the test mouse to freely explore for 10 min again. In the social novelty phase, a new stranger mouse was placed in the wire cage on the other side. Then, the test mice were allowed to freely explore for another 5 min. The interaction time (during which a mouse's nose touched the wire cup or was oriented toward the wire cup and came within 2 cm of it) was measured. The discrimination index was calculated by the formula (A-B)/(A + B). For sociability phase, A and B were defined as the interaction time with social wire cup and empty wire cup respectively; As for social novelty phase, A and B were defined as the interaction time with the cup of the novel stranger and the familiar one.

Statistical analysis

For all experiments, statistical analyses were performed with GraphPad Prism 8.01. Data represent mean ± SEM. Differences between two means were assessed by unpaired t-test. For comparing multiple measurements in the same experiment, data were analyzed by two-way ANOVA, and Bonferroni's tests were applied for multiple comparisons. Only values with $p < 0.05$ were accepted as statistically significant. Statistical details were provided in the figure legends.

Results

Pyramidal neurons (PNs) in dCA1 but not vCA1 are hyperexcitable in hAPP-J20 mice

We demonstrated previously that CA1 PNs were hyperactive in hAPP-J20 mice of 4–5 months old [42]. To further assess the properties of neurons in CA1, we crossed CaMKIIα-Cre or PV-Cre mice with hAPP-J20 mice and then injected rAAV-Ef1a-DIO-EYFP into the hippocampal CA1 region to visualize PNs and PV neurons, respectively (Fig. 1A). Results of whole-cell recordings showed that, in response to the depolarizing current injections, the spike numbers were increased in dCA1 PNs of 2.5-month-old hAPP-J20 mice (Fig. 1B), but the increase was more pronounced in dCA1 PNs of 6-month-old hAPP-J20 versus WT mice (Fig. 1C). However, no significant difference in spike numbers was observed in vCA1 PNs of 6-month-old hAPP-J20 versus WT mice (Fig. 1D). The spike numbers were also comparable in dCA1 PV^+ neurons between hAPP-J20 and WT mice at 6 months old (Fig. 1E). Furthermore, we measured the initial frequency (the frequencies of the first two action potentials) in response to the first suprathreshold current step to distinguish spiking from bursting. An increase in the mean initial frequency was found in the dCA1 PNs of 6-month-old hAPP-J20 mice (Fig. 1F, G), indicating a pronounced output mode transition of CA1 PNs from regular spiking to bursting. We also observed that the input resistance was significantly increased (Fig. 1H, I) but the rheobase was decreased (Fig. 1J) in dCA1 PNs of 6-month-old hAPP-J20 versus WT mice. The resting membrane potential (RMP) and the threshold to generate action potentials in dCA1 PNs were not significantly altered in hAPP-J20 mice (Fig. 1K, L). Taken together, our data demonstrated that the dCA1 PNs were hyperexcitable but the excitability of vCA1 PNs and PV^+ neurons in dCA1 was not significantly altered in 6-month-old hAPP-J20 mice.

Consistent with the hyperexcitability of dCA1 PNs in hAPP-J20 mice, we found that the frequency of the spontaneous action potentials (sAPs) was also increased in dCA1 PNs of hAPP-J20 versus WT mice (Fig. 1M, N).

Chemogenetic inhibition of dCA1 PNs ameliorated cognitive deficits in hAPP-J20 mice

Given that the hyperexcitability of dCA1 PNs may contribute to the behavioral deficits [42], we hypothesized that directly inhibiting hippocampal PNs might attenuate the behavioral deficits in hAPP-J20 mice. We first confirmed that our hAPP-J20 mice exhibited memory deficits in several behavioral tests (Fig. S1). We want to mention that an increased exploration distance was observed in hAPP-J20 mice in the novel location recognition test (Fig. S1E). This is consistent with previous studies showing that hAPP-J20 mice present increased

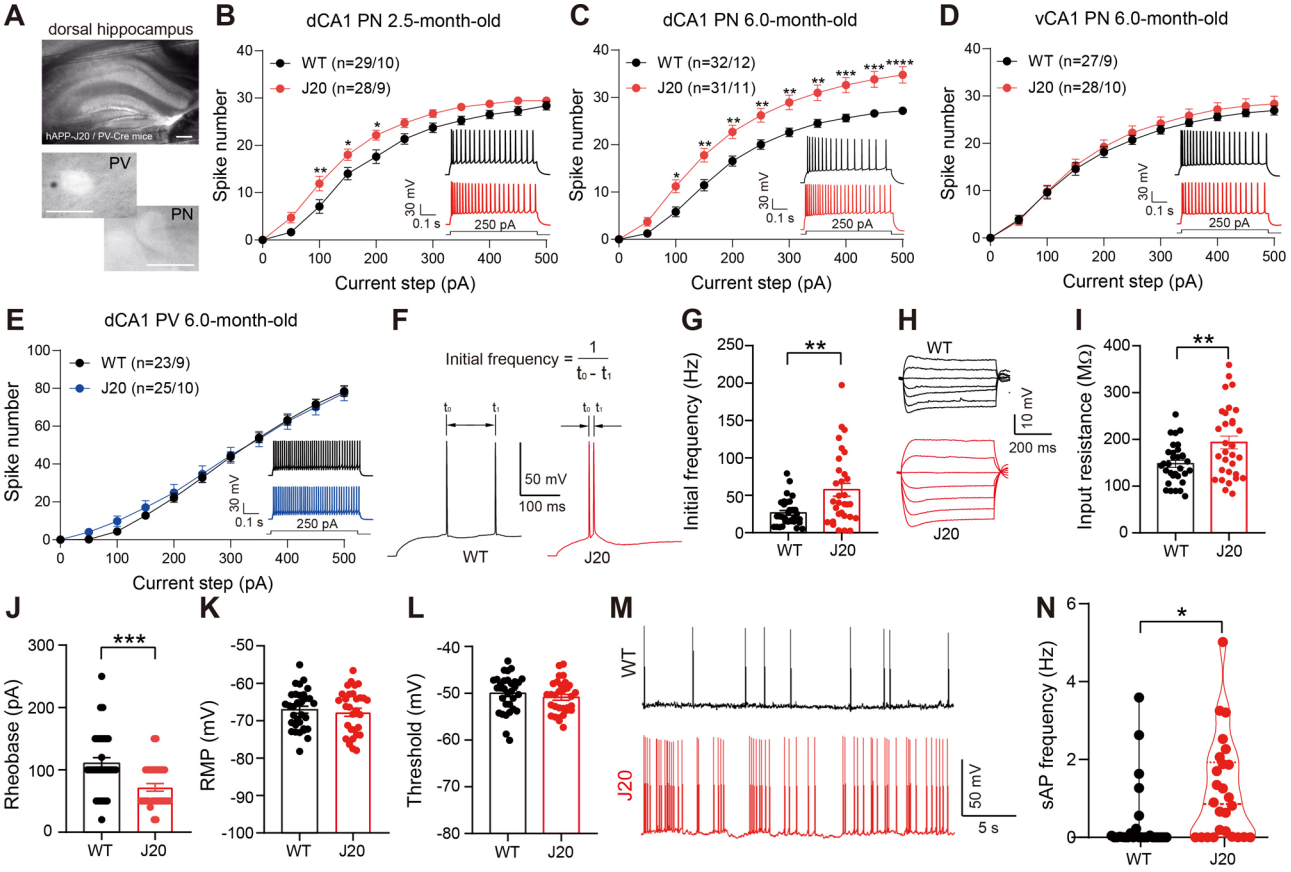

Fig. 1 Dorsal CA1 PNs are hyperexcitable in hAPP-J20 mice. (**A**) Images of brain slices showing the region of dorsal hippocampus (scale bar, 500 μm), a representative PV neuron and a representative pyramidal neuron (PN) (scale bars, 50 μm) for recordings. (**B**) The numbers of spikes generated in dCA1 PNs of WT and hAPP-J20 mice (2.5 months) in response to depolarizing current injections (WT, $n=29$ cells from 10 mice; J20, $n=28$ cells from 9 mice). Two-way ANOVA: genotype (hAPP), $F_{(1,55)}=6.503$, $p=0.0136$; current step, $F_{(10,550)}=557.3$, $p<0.0001$; interaction, $F_{(10,550)}=2.630$, $p=0.0039$; $^{*}p<0.05$, $^{**}p<0.01$ with Bonferroni's post-hoc test. (**C**) The numbers of spikes generated in dCA1 PNs of WT and hAPP-J20 mice (6 months) in response to depolarizing current injections (WT, $n=32$ cells from 12 mice; J20, $n=31$ cells from 11 mice). Two-way ANOVA: genotype (hAPP), $F_{(1,61)}=15.69$, $p=0.0002$; current step, $F_{(2.408,146.9)}=585.8$, $p<0.0001$; interaction, $F_{(10,610)}=5.962$, $p<0.0001$; $^{*}p<0.05$, $^{**}p<0.01$, $^{***}p<0.001$, $^{****}p<0.0001$ with Bonferroni's post-hoc test. (**D**) The numbers of spikes generated in vCA1 PNs of WT and hAPP-J20 mice (6 months) in response to depolarizing current injections (WT, $n=27$ cells from 9 mice; J20, $n=28$ cells from 10 mice). Two-way ANOVA with Bonferroni's post-hoc test: genotype (hAPP), $F_{(1,53)}=0.4698$, $p=0.4961$; current step, $F_{(2.426,128.6)}=411.6$, $p<0.0001$; interaction, $F_{(10,530)}=0.5348$, $p=0.8658$. (**E**) The numbers of spikes generated in dCA1 PV neurons of WT and hAPP-J20 mice (6 months) in response to depolarizing current injections (WT, $n=23$ cells from 9 mice; J20, $n=25$ cells from 10 mice). Two-way ANOVA with Bonferroni's post-hoc test: genotype (hAPP), $F_{(1,46)}=0.1271$, $p=0.7231$; current step, $F_{(1.944,89.41)}=630.8$, $p<0.0001$; interaction, $F_{(10,460)}=1.135$, $p=0.3342$. (**F**) Representative traces of the initial firing frequency in the dCA1 PNs of WT and hAPP-J20 mice (6 months). (**G**) Quantification of the initial frequency in the dCA1 PNs (WT, $n=32$ cells from 10 mice; J20, $n=31$ cells from 10 mice). Unpaired t-test: $t_{(61)}=3.392$, $p=0.0012$. $^{**}p<0.01$. (**H**) Representative traces of the input resistance in the dCA1 PNs of WT and hAPP-J20 mice (6 months). (**I**) Quantification of the input resistance in the dCA1 PNs (WT, $n=32$ cells from 10 mice; J20, $n=31$ cells from 10 mice). Unpaired t-test: $t_{(61)}=2.946$, $p=0.0046$. $^{**}p<0.01$. (**J**) The rheobase of dCA1 PNs in 6-month-old WT and hAPP-J20 mice (WT, $n=32$ cells from 10 mice; J20, $n=31$ cells from 10 mice). Unpaired t-test: $t_{(61)}=3.572$, $p=0.0007$. $^{***}p<0.001$. (**K**) The resting membrane potential (RMP) of dCA1 PNs in 6-month-old WT and hAPP-J20 mice (WT, $n=32$ cells from 10 mice; J20, $n=31$ cells from 10 mice). Unpaired t-test: $t_{(61)}=0.4743$, $p=0.6370$. (**L**) The threshold for generation of action potentials of dCA1 PNs in 6-month-old WT and hAPP-J20 mice (WT, $n=32$ cells from 10 mice; J20, $n=31$ cells from 10 mice). Unpaired t-test: $t_{(61)}=0.9104$, $p=0.3662$. (**M**) Representative traces of the spontaneous action potential (sAP) of dCA1 PNs in WT and hAPP-J20 mice (6 months). (**N**) Quantification of sAP in the dCA1 PNs (WT, $n=26$ cells from 10 mice; J20, $n=26$ cells from 10 mice). Unpaired t-test: $t_{(50)}=2.563$, $p=0.0134$

exploratory activity [41, 44–46]. To specifically inhibit the activity of dCA1 PNs, we took advantage of the DREADDs (designer receptors exclusively activated by designer drugs) approach [47]. Adeno-associated viruses (AAVs) expressing the Cre-dependent DREADD (pAAV-hSyn-DIO-hM4D(Gi)-mCherry) or a control vector (pAAV-hSyn-DIO-mCherry) were bilaterally injected into the dCA1 of hAPP-J20/CaMKIIα-Cre mice. As shown in Fig. 2A, the virus was mainly expressed in CA1 neurons. We performed electrophysiological recordings in brain slices to validate the effect of the Gi (hM4Di) DREADD on the activity of dCA1 PNs. Bath application of clozapine N-oxide (CNO) significantly decreased the activity of CA1 PNs (Fig. 2B), increased the rheobase

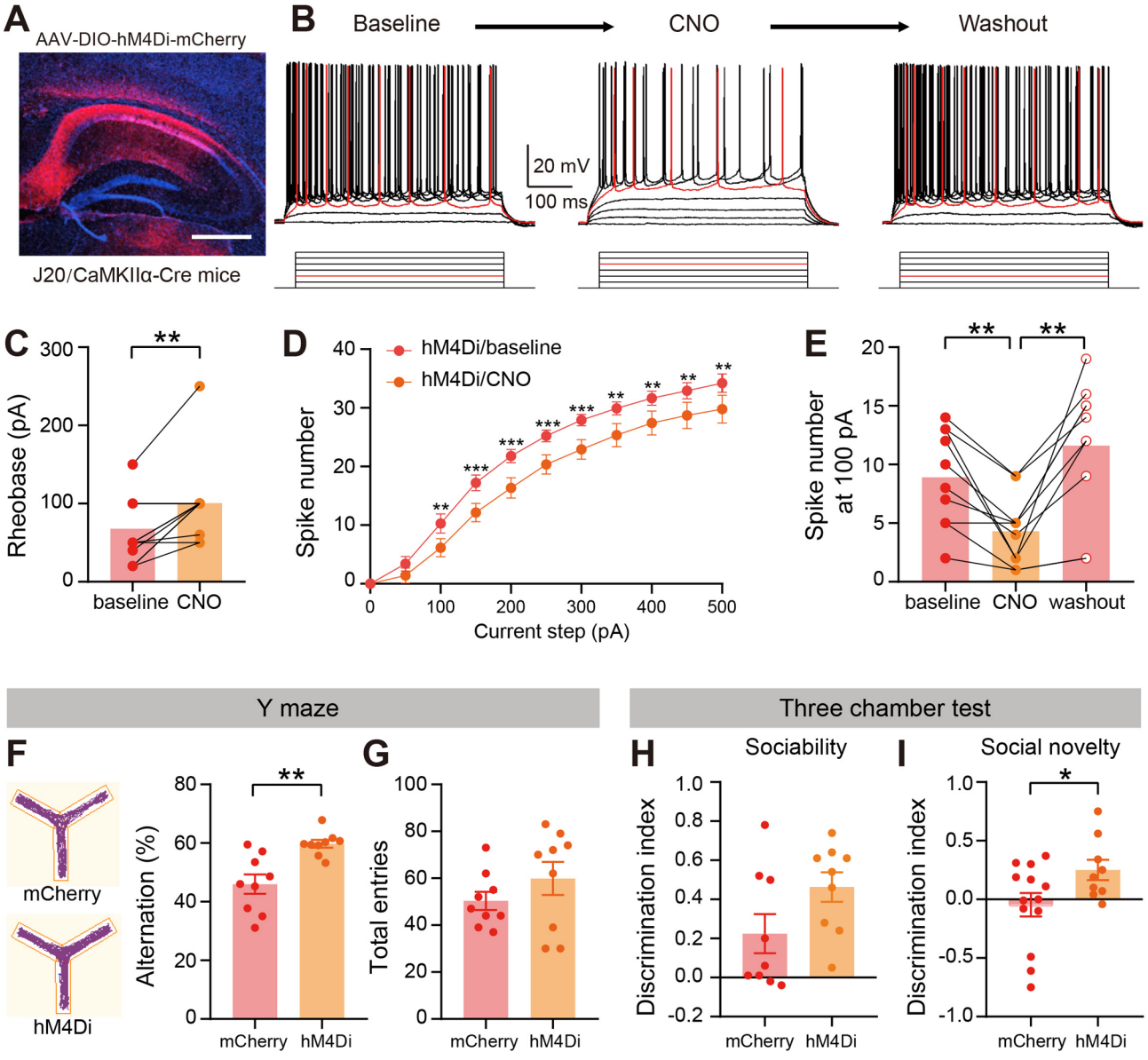

Fig. 2 Chemogenetic inhibition of dCA1 PNs improves cognitive functions of hAPP-J20 mice. (**A**) A representative image showing the expression of the AAV virus microinjected into the dCA1 of J20/CaMKIIα-Cre mice, red: mCherry, blue: DAPI. Scale bar, 500 μm. (**B**) Representative traces of action potentials recorded in dCA1 PNs before (baseline) and after bath application of CNO (10 μM) and washout of CNO. (Red traces represent the rheobase). (**C**) The rheobase of dCA1 PNs was higher after CNO treatment ($n = 11$ cells from 4 mice). Unpaired t-test: $t_{(10)} = 3.231$, $p = 0.0090$. $^{**}p < 0.01$. (**D**) The numbers of spikes generated in dCA1 PNs in response to depolarizing current injections were significantly decreased after CNO treatment ($n = 14$ cells from 5 mice). Two-way ANOVA: drug (CNO), $F_{(1, 13)} = 24.93$, $p = 0.0002$; current step, $F_{(10, 130)} = 125.5$, $p < 0.0001$; interaction, $F_{(10, 130)} = 2.957$, $p = 0.0022$; $^{**}p < 0.01$, $^{***}p < 0.001$ with Bonferroni's post-hoc test. (**E**) A summary plot in response to 100 pA depolarizing current step showing a significant decrease in the excitability of dCA1 PNs after CNO treatment ($n = 10$ cells from 4 mice). One-way ANOVA with Bonferroni's post-hoc test: $F_{(1.77, 15.93)} = 15.97$, $p = 0.0002$. $^{**}p < 0.01$. (**F**) Path traces of mice and the percentage of alternations in Y-maze test from hAPP-J20 mice expressing mCherry or hM4Di after CNO administration (mCherry, $n = 9$; hM4Di, $n = 9$). hAPP-J20 mice expressing hM4Di showed the increased alternations. Unpaired t-test: $t_{(16)} = 3.873$, $p = 0.0013$. $^{**}p < 0.01$. (**G**) The total arm entries of Y-maze test from hAPP-J20 mice expressing mCherry or hM4Di after CNO administration (mCherry, $n = 9$; hM4Di, $n = 9$). Unpaired t-test: $t_{(16)} = 0.1362$, $p = 0.8934$. (**H**) The sociability in three chamber tests from hAPP-J20 mice expressing mCherry or hM4Di after CNO administration (mCherry, $n = 9$; hM4Di, $n = 9$). Unpaired t-test: $t_{(16)} = 1.905$, $p = 0.0749$. (**I**) The social novelty in three chamber tests from hAPP-J20 mice expressing mCherry or hM4Di after CNO administration (mCherry, $n = 13$; hM4Di, $n = 9$). hAPP-J20 mice expressing hM4Di displayed an increased discrimination index compared with hAPP-J20 mice expressing mCherry. Unpaired t-test: $t_{(20)} = 2.107$, $p = 0.0479$. $^{*}p < 0.05$

(Fig. 2C) and decreased the firing rate of mCherry-positive neurons (Fig. 2D, E), confirming the inhibition of dCA1 PNs in hAPP-J20 mice. We conducted behavioral tests to assess the cognitive functions of mice. Our results showed that inhibiting dCA1 PNs for 2 weeks improved the performance of hAPP-J20 mice in both Y maze and three chamber tests (Fig. 2F-I), suggesting the cognitive functions were improved. Chemogenetic inhibition of dCA1 PNs for two weeks did not significantly affect the inflammation and Aβ deposition in the hippocampus of hAPP-J20 mice (Fig. S2).

Impaired HCN function in the dCA1 PNs of hAPP-J20 mice

HCNs are well known as pacemaker channels in maintaining spontaneous rhythmic activity and regulating neuronal excitability [21], and HCN1 and HCN2 are highly expressed in the hippocampal PNs [23, 25]. We wondered whether the hyperexcitability of dCA1 PNs in hAPP-J20 mice was associated with the dysregulated HCNs. To examine the function of HCN channels in dCA1 PNs of hAPP-J20 mice, we performed whole-cell voltage clamping to directly measure the HCN channel-mediated currents (I_h) in dCA1 PNs by holding the membrane voltage from −45 to -105 mV in 10-mV steps. We found that the sag ratio and amplitude (Fig. 3A-C) and the I_h currents (Fig. 3D, E) were significantly reduced in dCA1 PNs of 6-month-old hAPP-J20 versus WT mice, suggesting impaired functions of HCNs in the dCA1 PNs of hAPP-J20 mice. Our results showed that there was no difference in the sag ratio, amplitude and the I_h currents in the dCA1 PV neurons between WT and hAPP-J20 mice (Fig. 3F-J).

Aβ disrupts the functions of HCN channels

Besides Aβ, hAPP is also overexpressed in the hippocampus of hAPP-J20 mice [36]. To determine whether the high level of Aβ affects the function of HCNs or not, we prepared acute brain slices from WT mice and incubated the slices with oligomeric Aβ (Fig. 3K). Whole cell recordings in dCA1 PNs showed that the amplitudes of I_h were significantly reduced after treatment with Aβ (Fig. 3L, M), suggesting that Aβ disrupted the function of HCNs in dCA1 PNs. Interestingly, treatment with cAMP, a facilitator of HCNs, reversed the effect of Aβ on the amplitudes of I_h in dCA1 PNs (Fig. 3L, M).

Impaired HCN contributes to the hyperexcitability of dCA1 PNs in hAPP-J20 mice

To investigate whether the impaired function of HCN channels is associated with the hyperexcitability of dCA1 PNs of hAPP-J20 mice, we first recorded the I_h currents in dCA1 PNs in the presence of 8-Br-cAMP (1 mM in the pipette), an analog of cAMP which is a facilitator of HCN channels [48, 49]. Reduced levels of cAMP were reported in the cortex of 5×FAD mice [50] and we found that the level of cAMP measured with ELISA was significantly decreased in the hippocampus of 6-month-old hAPP-J20 versus WT mice (Fig. 4A). Interestingly, incubation with 8-Br-cAMP significantly enhanced the I_h currents in dCA1 PNs (Fig. 4B, C) and decreased the number of the spikes in response to depolarizing current injections (Fig. 4D, E) in dCA1 PNs of 6-month-old hAPP-J20 mice. Similarly, bath application of brain slices with ZD7288, a selective inhibitor of HCN channels [51], led to a progressive and significant increase in the firing rate in dCA1 PNs of hAPP-J20 and WT mice (Fig. 5A, B). These results indicated that the disrupted function of HCNs is associated with the hyperexcitability of dCA1 PNs in hAPP-J20 mice. We noted, however, that cAMP decreased firing frequency at high stimulation rates but did not shift the firing curve at lower frequencies (Fig. 4E), suggesting that cAMP may act through other cAMP-dependent pathways beyond HCN channel activation to regulate the excitability of CA1 PNs. We also noted the persistence of the original firing rate difference between WT and hAPP-J20 mice following ZD7288 application (Fig. 5), suggesting that HCN channel activity alone does not fully account for the difference in excitability of CA1 PNs between WT and J20 mice.

The expression of HCN2 is reduced in the hippocampal membrane extractions of hAPP-J20 mice

HCN channels include 4 subtypes: HCN1, HCN2, HCN3 and HCN4[21]. Among these four subtypes, HCN1 and HCN2 are the major subtypes predominantly expressed in the hippocampal pyramidal neurons [23, 24]. To investigate which subtype(s) of HCNs may contribute to the disrupted function of HCNs in dCA1 of hAPP-J20 mice, we examined the expression of HCN1 and HCN2 in the hippocampus of 5–6 months old WT and hAPP-J20 mice. Results of immunohistochemical staining showed that the expression pattern of HCN1 and HCN2 was similar, with weak expression in the pyramidal layer of CA1-CA3, moderate expression in the SR (stratum radiatum) and OR (stratum oreins) of CA1, and intense expression in the SLM (stratum lacunosum-molecularis) of CA1 (Fig. S3A and Fig. S4A), although the expression of HCN1 was slightly stronger in the pyramidal layer of CA1-CA3 than that of HCN2 (Fig. S3C and Fig. S4C). These results are consistent with the notion that HCN1 and HCN2 are accumulated in the distant dendritic fragments of hippocampal pyramidal neurons [23]. The expression of both HCN1 and HCN2 was very weak in the granule layer and molecular layer of the DG (Fig. S3A and Fig. S4A). We quantified the relative density of HCN1 and HCN2 in the SLM and our results showed that the expression level of HCN1 was similar in the SLM of WT and hAPP-J20 mice (Fig. S3D, E), but the level of HCN2 was reduced in the

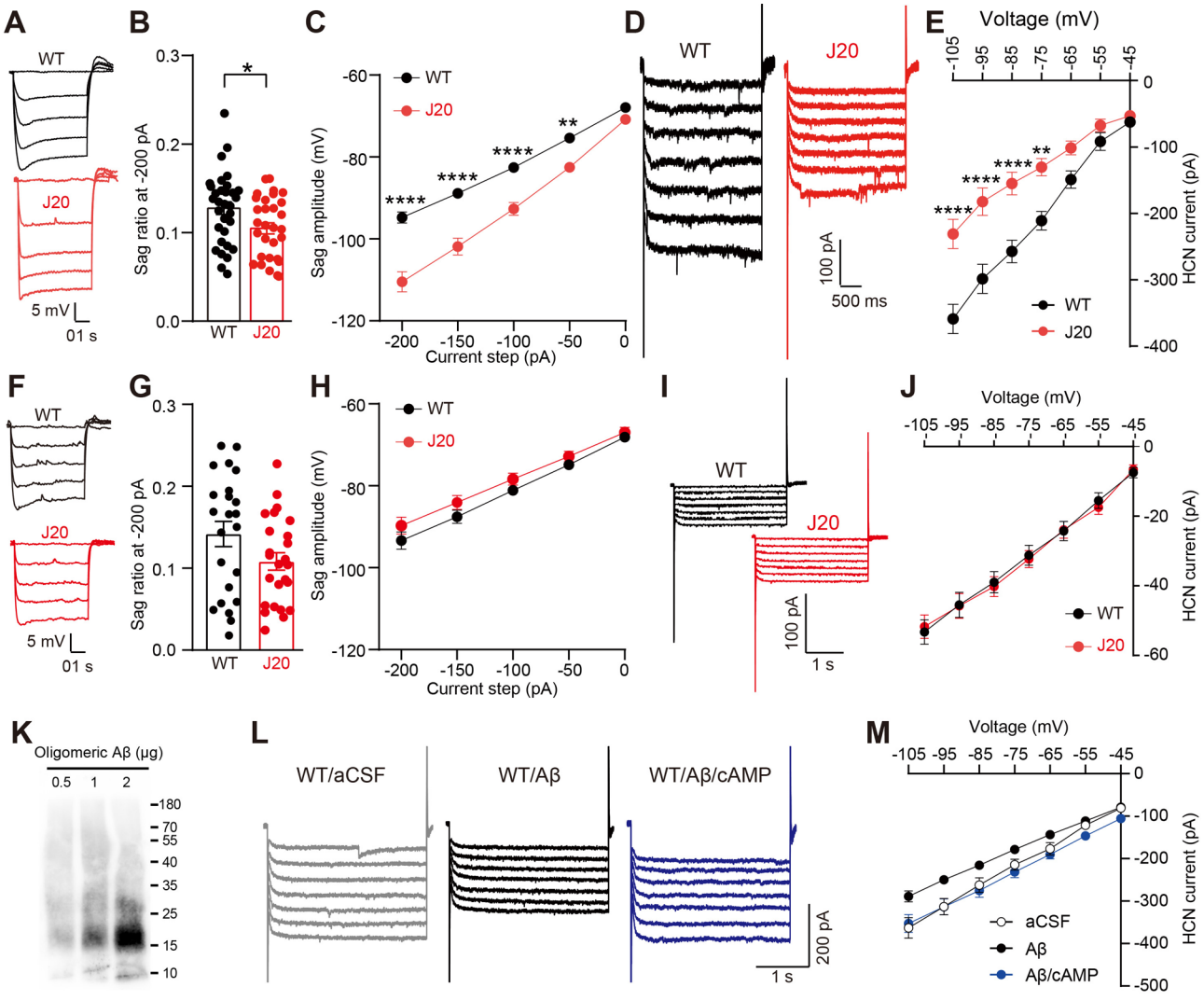

Fig. 3 Disrupted functions of HCNs in dCA1 PNs of hAPP-J20 mice or in dCA1 PNs of WT mice treated with oligomeric Aβ. **(A)** Representative traces elicited by a series of negative current injections of dCA1 PNs in WT and hAPP-J20 mice. (**B**) The sag ratio at the − 200 pA current injection detected from the dCA1 PNs of hAPP-J20 and WT mice. Unpaired t-test: $t_{(61)} = 2.395$, $p = 0.0197$. (**C**) Sag amplitudes of dCA1 PNs at − 200 to 0-pA current injections. Two-way ANOVA: genotype (hAPP), $F_{(1, 61)} = 31.81$, $p < 0.0001$; current step, $F_{(1.225, 74.71)} = 450.0$, $p < 0.0001$; interaction, $F_{(4, 244)} = 16.29$, $p < 0.0001$; $^{**}p < 0.01$, $^{****}p < 0.0001$ with Bonferroni's post-hoc test. (**D**) Representative traces of the HCN-conducted I_h currents in dCA1 PNs of WT and hAPP-J20 mice. (**E**) The HCN-conducted I_h currents in dCA1 PNs of hAPP-J20 and WT mice (WT, $n = 10$ cells from 5 mice; J20, $n = 10$ cells from 5 mice). Two-way ANOVA: genotype (hAPP), $F_{(1, 18)} = 18.04$, $p = 0.0005$; voltage step, $F_{(6, 108)} = 124.7$, $p < 0.0001$; interaction, $F_{(6, 108)} = 8.998$, $p < 0.0001$; $^{**}p < 0.01$, $^{****}p < 0.0001$ with Bonferroni's post-hoc test. (**F**) Representative traces elicited by a series of negative current injections of dCA1 PVs in WT and hAPP-J20 mice. (**G**) The sag ratio at the − 200 pA current injection detected from the dCA1 PVs of hAPP-J20 and WT mice. Unpaired t-test: $t_{(46)} = 1.812$, $p = 0.0765$. (**H**) The sag amplitudes of PVs from hAPP-J20 and WT mice. Two-way ANOVA: genotype (hAPP), $F_{(1, 46)} = 2.134$, $p = 0.1508$; current step, $F_{(1.025, 47.16)} = 243.4$, $p < 0.0001$; interaction, $F_{(4, 184)} = 0.7310$, $p = 0.5719$. (**I**) Representative traces of the HCN-conducted I_h currents in dCA1 PVs of WT and hAPP-J20 mice. (**J**) The HCN-conducted I_h currents of dCA1 PVs of hAPP-J20 and WT mice (WT, $n = 23$ cells from 9 mice; J20, $n = 25$ cells from 10 mice). Two-way ANOVA: genotype (hAPP), $F_{(1, 23)} = 0.005643$, $p = 0.9408$; voltage step, $F_{(2.001, 46.03)} = 224.3$, $p < 0.0001$; interaction, $F_{(6, 138)} = 0.3319$, $p = 0.9192$. (**K**) Representative bands showing the Aβ oligomers by western blotting with 6E10. (**L**) Representative traces of the HCN-conducted I_h currents in dCA1 PNs of WT mice sampled from baseline, Aβ oligomers (10 nM) and Aβ + cAMP treatment, respectively. **(M)** Quantification of the I_h currents in dCA1 PNs from the three groups in (L) (baseline, $n = 15$ cells from 5 mice; Aβ, $n = 15$ cells from 5 mice; Aβ + cAMP, $n = 14$ cells from 5 mice). Two-way ANOVA with Bonferroni's post-hoc test: drug, $F_{(2, 41)} = 5.383$, $p = 0.0084$; voltage step, $F_{(6, 246)} = 506.2$, $p < 0.0001$; interaction, $F_{(12, 246)} = 3.875$, $p < 0.0001$

SLM of hAPP-J20 versus WT mice (Fig. 6A, B). In the neocortex, the expression of HCN1 was mainly found in the soma of layer 5 neurons and in the distant dendritic fragments of superficial layers (Fig. S3A, B), which is consistent with previous reports [23]. The expression of HCN2 was observed in cells distributed in different layers of the neocortex (Fig. S4A). However, we did not find intense expression of HCN2 in the distal dendrites in the neocortex (Fig. S4A, B), which is different from the data of previous reports [23].

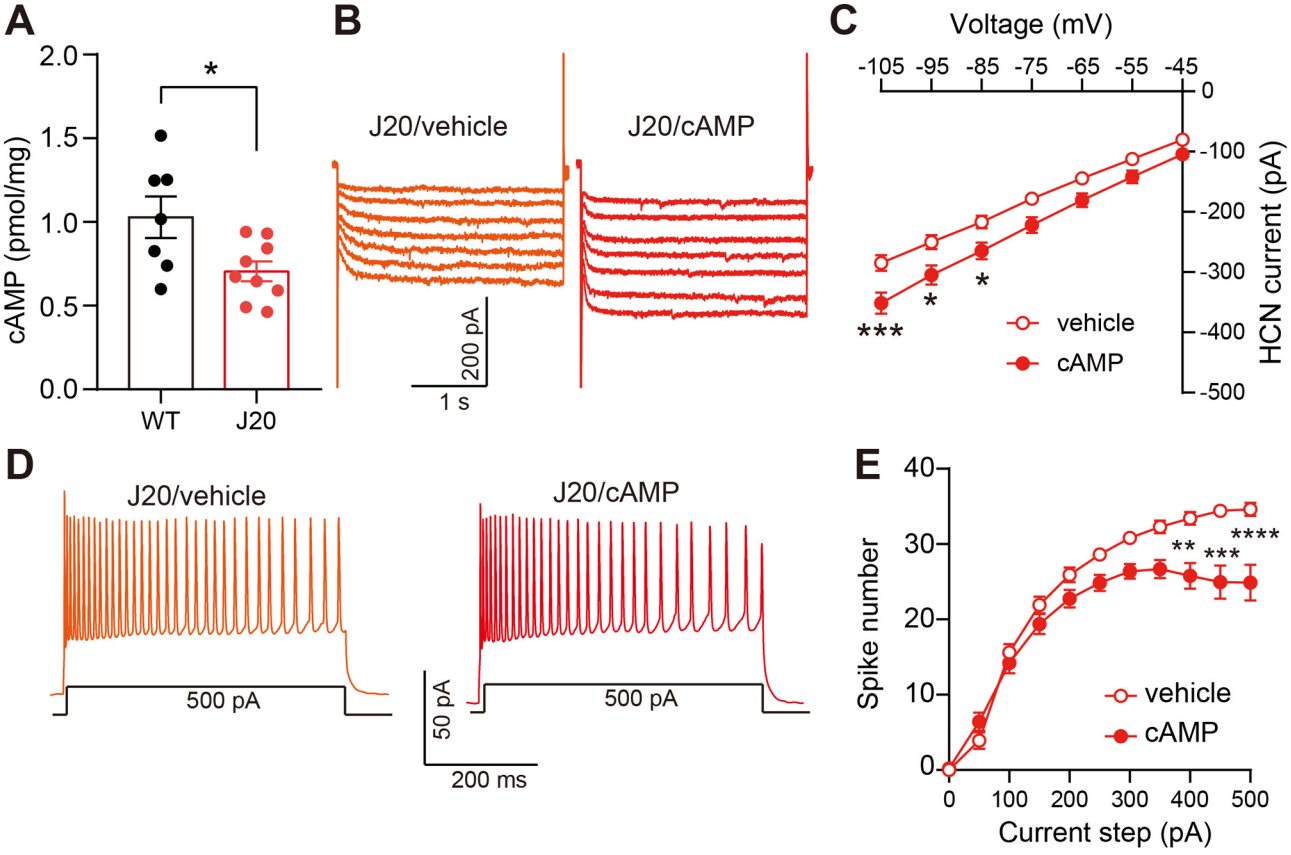

Fig. 4 Activating HCN channels by cAMP decreases the hyperexcitability of dCA1 PNs in hAPP-J20 mice. (**A**) Levels of cAMP in the hippocampus of WT and hAPP-J20 mice (WT, $n=7$; J20, $n=9$). Unpaired t-test: $t_{(14)}=2.539$, $p=0.0236$. *$p<0.05$. (**B**) Representative traces of the HCN-conducted I_h currents in the dCA1 PNs of 8-Br-cAMP- (1mM in the pipette) or vehicle-treated brain slices from hAPP-J20 mice. (**C**) Quantification of the I_h currents in the dCA1 PNs (vehicle, $n=19$ cells from 7 mice; cAMP, $n=23$ cells from 8 mice). Two-way ANOVA: drug, $F_{(1, 40)}=7.384$, $p=0.0097$; voltage step, $F_{(6, 240)}=642.5$, $p<0.0001$; interaction, $F_{(6, 240)}=5.266$, $p<0.0001$; *$p<0.05$, ***$p<0.001$ with Bonferroni's post-hoc test. (**D**) Sample traces of action potentials obtained at the 500 pA current injection in the dCA1 PNs of 8-Br-cAMP- or vehicle-treated brain slices from hAPP-J20 mice. (**E**) Quantification of the spike numbers in dCA1 PNs (vehicle, $n=10$ cells from 4 mice; cAMP, $n=19$ cells from 6 mice). Two-way ANOVA: drug, $F_{(1, 27)}=8.043$, $p=0.0086$; current step, $F_{(1.539, 41.56)}=165.6$, $p<0.0001$; interaction, $F_{(10, 270)}=5.481$, $p<0.0001$; **$p<0.01$, ***$p<0.001$, ****$p<0.0001$ with Bonferroni's post-hoc test

To further examine the expression of HCN1 and HCN2 in the hippocampus of WT and hAPP-J20 mice, we performed western blot analysis. When the lysates of the whole hippocampal tissue were used for the analysis, no difference in the expression levels of both HCN1 and HCN2 was found between WT and hAPP-J20 mice (Fig. S3F, G and Fig. S4D, E), which is consistent with a previous study [30]. However, the expression of HCN2 but not HCN1 was reduced in the hippocampal membrane extractions of hAPP-J20 versus WT mice (Fig. 6C-E). These data suggest that the reduced expression of HCN2 in the membrane extractions of the hippocampus may be one of the factors accounting for the impaired function of HCNs in dCA1 PNs of hAPP-20 mice.

The expression of HCN2 is reduced in CA1 of AD patients

Previous studies reported that the expression of HCN1 detected with western blot or proteomics was reduced in the temporal lobe of AD patients [27]. However, this reduction of HCN1 could be due to loss of neurons but not the reduced expression of HCN1 in individual neurons. A recent study reported that the expression of both HCN1 and HCN2 was increased in the hippocampus of patients with AD [33]. To further examine whether the expression of HCN2 is altered in the hippocampus of AD patients, we performed immunohistochemical staining. Our results showed that, unlike the intensive expression in the SLM of CA1 in mice (Fig. S3A and Fig. S4A), the expression of HCN2 was mainly observed in the soma but not the distant fragments of the neuronal dendrites in the human hippocampus (Fig. S5 and Fig. S6). On the other hand, the expression of HCN2 were widely expressed in neurons across the whole hippocampus including the pyramidal layer of CA1-CA3, the granule layer of DG and the polymorphic layer of DG (Fig. S5 and Fig. S6). Our quantification data revealed that the overall density of the HCN2 expression was reduced in the CA1 field of AD patients versus non-AD controls (Fig. 6F, G).

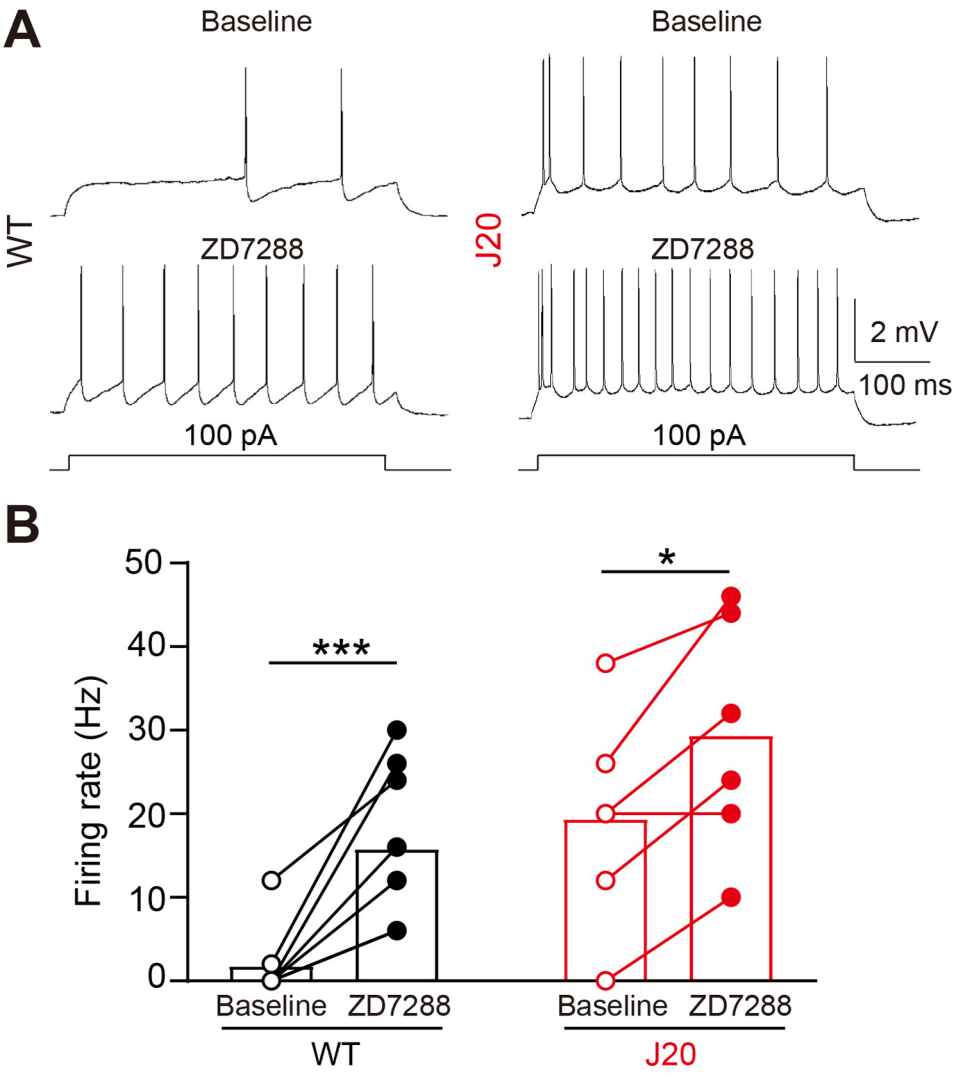

Fig. 5 Blocking HCN channels leads to increased excitability of dCA1 PNs in WT and hAPP-J20 mice. (**A**) Representative traces of action potentials in the dCA1 PNs of baseline or ZD7288 (10 μM)-treated brain slices from WT and hAPP-J20 mice. (**B**) Summary graph of the firing rate of dCA1 PNs before and after ZD7288 treatment in WT and hAPP-J20 mice (WT, $n=8$ cells from 3 mice; J20, $n=6$ cells from 3 mice). Two-way ANOVA: genotype (hAPP), $F_{(1,12)}=8.978$, $p=0.0111$; drug (ZD7288), $F_{(1,12)}=30.86$, $p=0.0001$; interaction, $F_{(1,12)}=0.8571$, $p=0.3728$; *$p<0.05$, ***$p<0.001$ with Bonferroni's post-hoc test

However, the overall reduction of HCN2 in CA1 could be related with the less density of neurons in CA1 of AD patients. Therefore, we further quantified the expression of HCN2 in individual CA1 neurons. We found that the expression of HCN2 was reduced in individual CA1 neurons of AD patients versus no-AD controls, as well (Fig. 6H, I).

The expression pattern of HCN1 in the hippocampus of humans is very similar to that of HCN2 (Fig. S7). Unfortunately, we were not able to obtain further samples from AD patients to compare the expression of HCN1 in the hippocampus between AD and non-AD controls.

Overexpression of HCN2 attenuates the excitability of dCA1 PNs, enhances the CA1 LTP and improves cognitive functions of hAPP-J20 mice

Although cAMP is known to increase the I_h currents [49], the effect of cAMP on HCN channels is nonselective. Based on our data that the function of HCNs was impaired in dCA1 PNs of hAPP-J20 mice (Fig. 3) and the expression of HCN2 was reduced in the CA1 neurons of both AD patients and AD mice (Fig. 6), we wondered whether overexpressing HCN2 in dCA1 PNs could rescue the function of HCNs. To restore the expression of HCN2 specifically in CA1 PNs of hAPP-J20 mice, rAAV-CaMKIIα-HCN2-P2A-EGFP-WPREs (rAAV-CaMKIIα-EGFP was used as the control) was injected bilaterally into the dCA1 of WT and hAPP-J20 mice. As

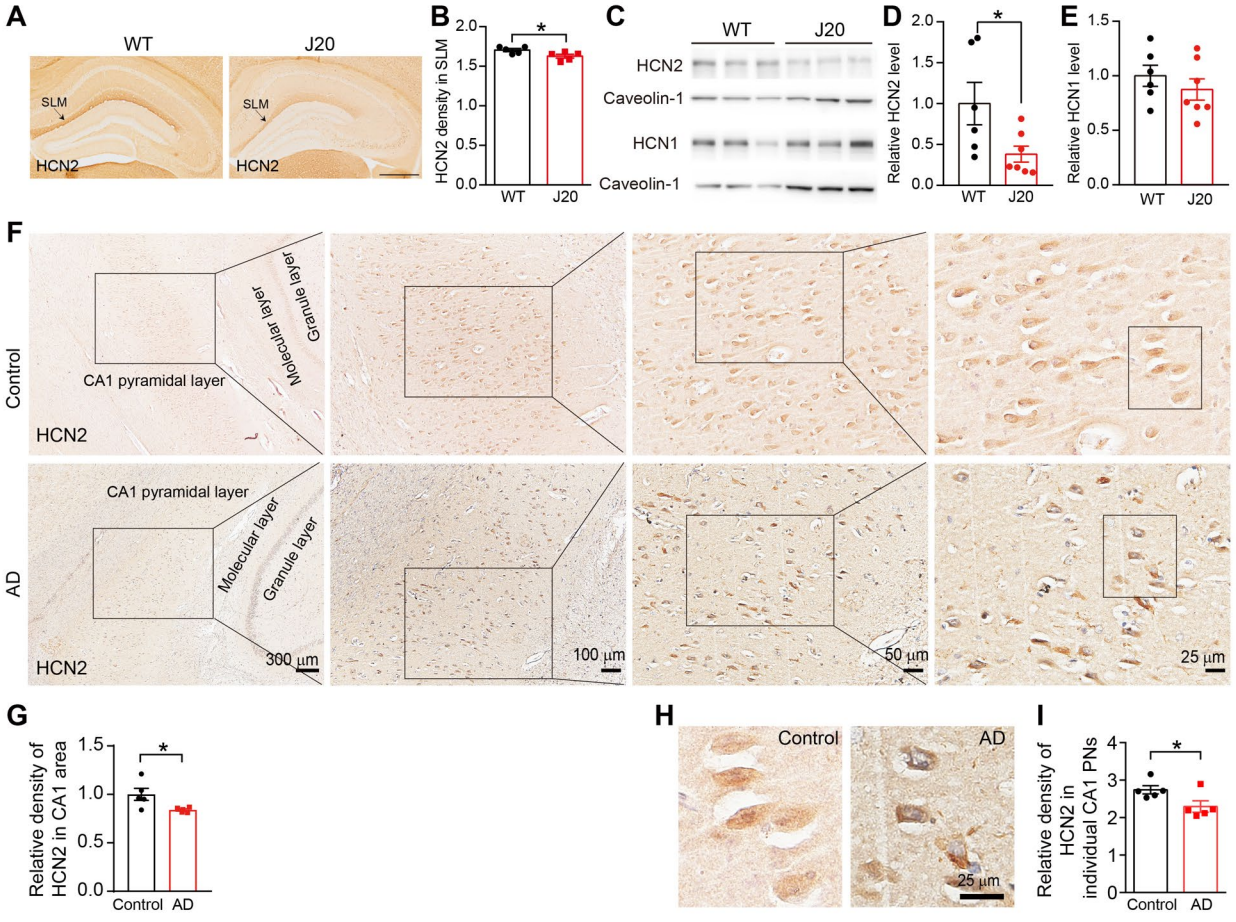

Fig. 6 Expression of HCN2 is reduced in CA1 PNs of hAPP-J20 mice and AD patients. (**A**) Representative images showing the expression of HCN2 in the hippocampus of 6-month-old WT and hAPP-J20 mice. Scale bar, 500 μm. (**B**) Quantification of the HCN2 expression in the SLM of CA1 of WT ($n=5$) and hAPP-J20 mice ($n=5$). Unpaired t-test: $t_{(8)}=2.473$, $p=0.0385$. *$p<0.05$, statistical power = 0.68. (**C**) Protein bands of HCN2 and HCN1 in the hippocampal membranous fractions of WT and hAPP-J20 mice, caveolin-1 severed as the loading control. (**D**) Quantification of the levels of HCN2 in the hippocampal membranous fractions of WT ($n=6$) and hAPP-J20 mice ($n=7$). Unpaired t-test: HCN2: $t_{(11)}=2.372$, $p=0.0370$. *$p<0.05$. (**E**) Quantification of the levels of HCN1 in the hippocampal membranous fractions of WT ($n=6$) and hAPP-J20 mice ($n=7$). Unpaired t-test: HCN1: $t_{(11)}=0.9095$, $p=0.3826$. (**F**) Representative images showing the expression of HCN2 in the hippocampus of AD patients and non-AD controls. (**G**) Quantification data revealed that the overall density of the HCN2 was decreased in the CA1 area of AD patients ($n=5$) versus non-AD controls ($n=5$). Unpaired t-test: HCN1: $t_{(8)}=2.567$, $p=0.0333$. *$p<0.05$. (**H**) Representative images showing the expression of HCN2 in individual CA1 neurons of AD patients and no-AD controls (from the boxes shown in the far right part of F). Scale bar, 25 μm. (**I**) Quantification data revealed that the expression of HCN2 was decreased in individual CA1 PNs of AD patients ($n=5$) versus non-AD controls ($n=5$). Unpaired t-test: HCN1: $t_{(8)}=2.360$, $p=0.046$. *$p<0.05$

shown in Fig. 7A-C, the virus was efficiently expressed in dCA1 PNs, and the expression of HCN2 was increased 3 weeks after the injection of the virus. Whole cell recordings revealed that overexpressing HCN2 increased the sag ratio and amplitude (Fig. 7D-F) and the I_h currents (Fig. 7H, I) in dCA1 PNs of hAPP-J20 mice. More importantly, overexpressing HCN2 decreased the input resistance (Fig. 7J) and the number of spikes generated in dCA1 PNs of hAPP-J20 mice in response to the depolarizing current injections (Fig. 7K, L), suggesting that the excitability of dCA1 PNs was reduced. Single cell capacitance was measured to confirm that the recorded cells are PNs (Table S1). Overexpressing HCN2 also significantly decreased the frequency of spontaneous APs in CA1 PNs of hAPP-J20 mice (Fig. 7M, N). These results suggested that the reduction of HCN2 was associated with the hyperexcitability of CA1 PNs in hAPP-J20 mice.

We also prepared acute brain slices and performed field recordings in CA1 to measure the long-term potentiation (LTP). Our results showed that overexpressing HCN2 significantly enhanced the CA1 LTP at the Schaffer collateral inputs of hAPP-J20 mice (Fig. 7O, P).

We then performed behavioral tests to assess the effects of overexpressing HCN2 in dCA1 PNs on the cognitive functions of hAPP-J20 mice. The spatial learning and memory that mainly related to dorsal hippocampus were assessed by the Y maze test. We found that the memory was impaired in J20 mice, and overexpressingHCN2

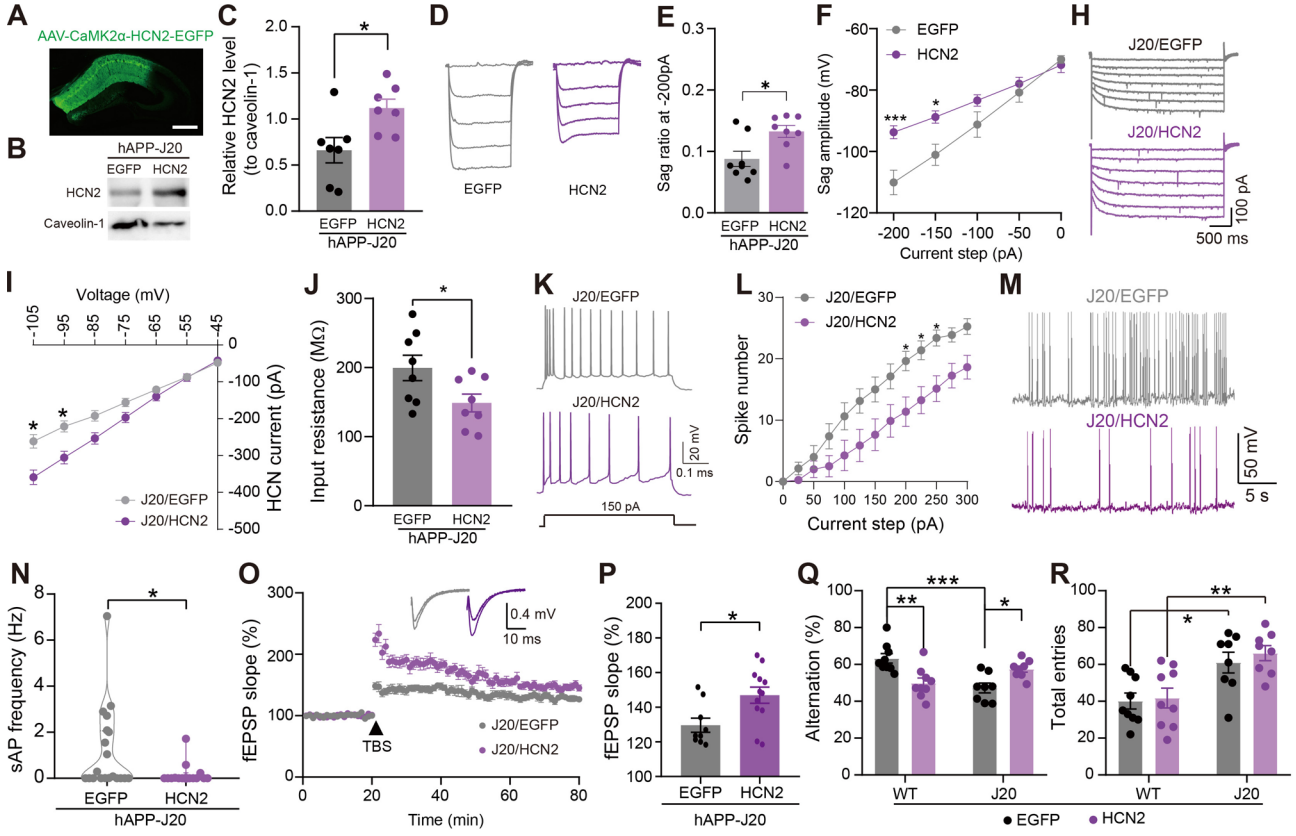

Fig. 7 Overexpressing HCN2 enhances the activity of HCNs, decreases the excitability of dCA1s, increases the CA1 LTP and improves cognitive functions in hAPP-J20 mice. (**A**) Representative images showing the expression of the virus microinjected in the dCA1 of hAPP-J20 mice. Scale bar, 500 μm. (**B**) Representative bands of HCN2 in western blottings of the hippocampal tissues from hAPP-J20 mice with or without overexpressing HCN2. (**C**) Quantification of the relative HCN2 levels in the hippocampus (EGFP, $n=7$; HCN2, $n=7$). Unpaired t-test: $t_{(12)}=2.718$, $p=0.0187$. *$p<0.05$. (**D**) Representative traces elicited by a series of negative current injections of dCA1 PNs in hAPP-J20 mice with (HCN2) or without (EGFP) overexpression of HCN2. (**E**) The sag ratios detected in dCA1 PNs of hAPP-J20 mice with HCN2 overexpression ($n=8$) or without HCN2 overexpression ($n=8$). Unpaired t-test: $t_{(15)}=2.182$, $p=0.0454$. *$p<0.05$. (**F**) Sag amplitudes of dCA1 PNs in hAPP-J20 mice with or without overexpressing HCN2 at −200 to 0-pA current injections. Two-way ANOVA: virus (HCN2), $F_{(1, 14)}=4.448$, $p=0.0534$; current step, $F_{(1.612, 22.57)}=150.8$, $p<0.0001$; interaction, $F_{(4, 56)}=13.14$, $p<0.0001$; *$p<0.05$, ***$p<0.001$ with Bonferroni's post-hoc test. (**H**) Representative traces of the HCN-conducted I_h currents in the dCA1 PNs with or without overexpressing HCN2. (**I**) Quantification of the I_h currents (EGFP, $n=8$ cells from 4 mice; HCN2, $n=8$ cells from 4 mice). Two-way ANOVA: virus (HCN2), $F_{(1, 15)}=6.178$, $p=0.0252$; voltage step, $F_{(1.314, 19.71)}=533.1$, $p<0.0001$; interaction, $F_{(6, 90)}=23.46$, $p<0.0001$; *$p<0.05$ with Bonferroni's post-hoc test. (**J**) The input resistance was significantly decreased in dCA1 PNs of hAPP-J20 mice after overexpressing HCN2 (EGFP, $n=8$ cells from 4 mice; HCN2, $n=8$ cells from 4 mice). Unpaired t-test: $t(14)=2.249$, $p=0.0411$. *$p<0.05$. (**K**) Sample traces of action potentials in dCA1 PNs of hAPP-J20 mice with or without HCN2 overexpression obtained at the 150 pA current injection. (**L**) Quantifications of the spike numbers of dCA1 PNs in response to current injections (EGFP, $n=8$ cells from 4 mice; HCN2, $n=8$ cells from 4 mice). Two-way ANOVA: virus (HCN2), $F_{(1, 14)}=6.597$, $p=0.0223$; current step, $F_{(2.272, 31.80)}=107.9$, $p<0.0001$; interaction, $F_{(12, 168)}=3.584$, $p<0.0001$; *$p<0.05$ with Bonferroni's post-hoc test. **(M)** Representative traces of sAP of dCA1 PNs in hAPP-J20 with or without HCN2 overexpression. **(N)** Frequency of sAP in the dCA1 PNs of hAPP-J20 mice with or without HCN2 overexpression (EGFP, $n=20$ cells from 8 mice; HCN2, $n=15$ cells from 7 mice). Unpaired t-test: $t_{(33)}=2.047$, $p=0.0487$. *$p<0.05$. **(O)** Representative traces showing LTP in CA1 of hAPP-J20 with or without HCN2 overexpression. **(P)** Quantification of the last 15 min of the fEPSP recordings (EGFP, $n=9$ cells from 5 mice; HCN2, $n=12$ cells from 5 mice). Unpaired t-test: $t_{(19)}=2.683$, $p=0.0147$. *$p<0.05$. **(Q)** The percentage of alternations in Y-maze test from WT and hAPP-J20 mice with or without overexpressing HCN2 (WT/EGFP: $n=9$; WT/HCN2: $n=9$; J20/EGFP: $n=8$; J20/HCN2: $n=8$). Two-way ANOVA: genotype (hAPP), $F_{(1,30)}=2.938$, $p=0.0969$; virus (HCN2), $F_{(1,30)}=0.4145$, $p=0.5246$; interaction, $F_{(1,30)}=22.76$, $p<0.0001$; *$p<0.05$, **$p<0.01$, ***$p<0.001$ with Bonferroni's post-hoc test. **(R)** The total arm entries in the Y-maze test from WT and hAPP-J20 mice with or without overexpressing HCN2 (WT/EGFP: $n=9$; WT/HCN2: $n=9$; J20/EGFP: $n=8$; J20/HCN2: $n=8$). Two-way ANOVA: genotype (hAPP), $F_{(1,30)}=21.32$, $p<0.0001$; virus (HCN2), $F_{(1,30)}=0.4806$, $p=0.4935$; interaction, $F_{(1,30)}=0.1246$, $p=0.7266$; *$p<0.05$, **$p<0.01$ with Bonferroni's post-hoc test

improved the memory of hAPP-J20 mice (Fig. 7Q) without affecting the total entries in the Y maze test (Fig. 7R). Our data also showed that overexpressing HCN2 in dCA1 impaired the memory of WT mice but did not affect their total entries in the Y maze test (Fig. 7Q, R).

Knocking down the expression of HCN2 in CA1 PNs reduces the activity of HCNs, increases the excitability of CA1 PNs and impairs the cognitive functions of WT mice

We have shown that reduction of HCN2 was associated with the hyperexcitability of dCA1 PNs and the impaired cognition of hAPP-J20 mice. To further evaluate the roles

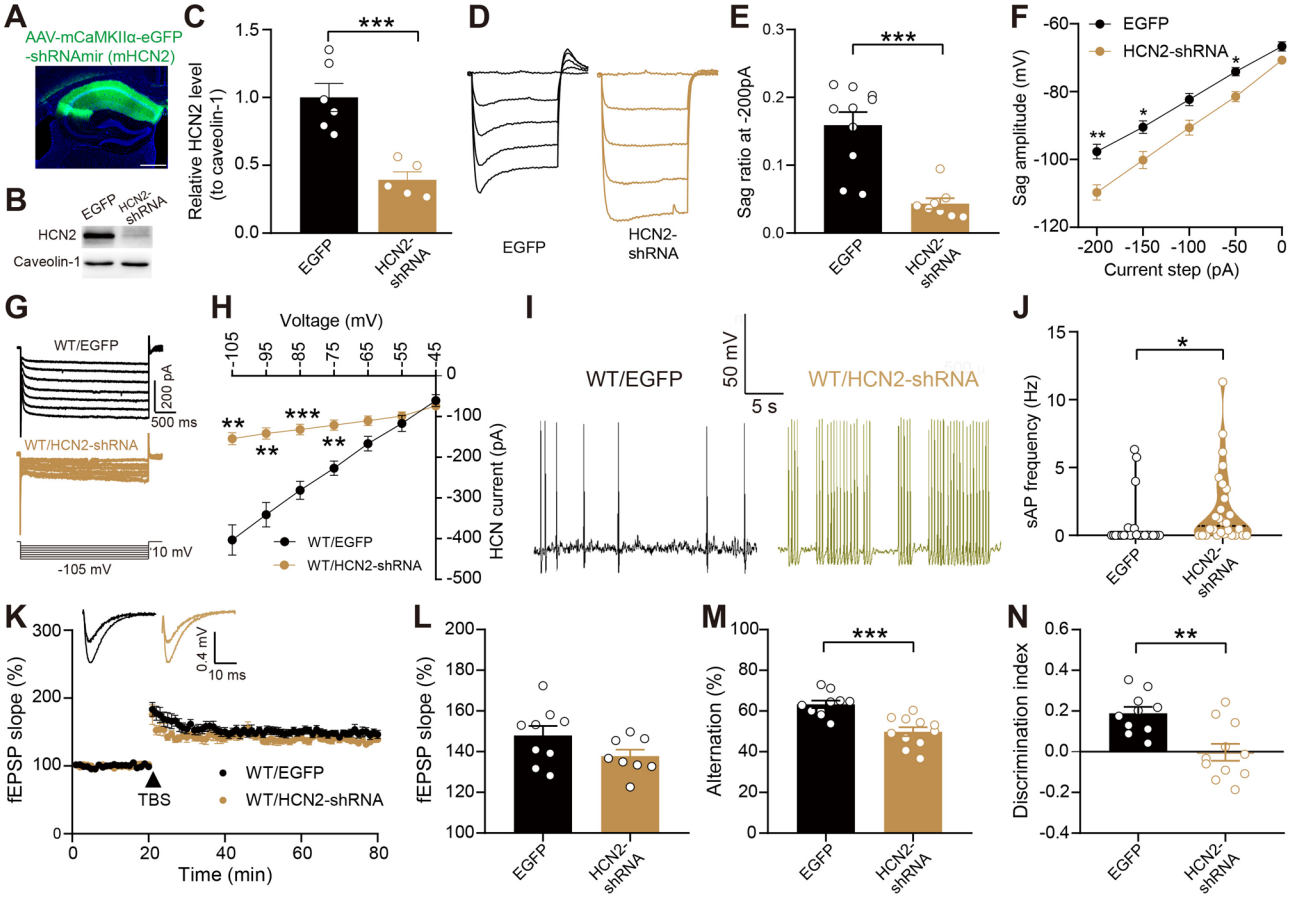

Fig. 8 Knocking down the expression of HCN2 decreases the activity of HCNs, increases the excitability of dCA1s and impairs cognitive functions in WT mice. (**A**) Representative images showing the expression of the AAV virus microinjected into the dCA1 of WT mice. Scale bar, 500 μm. (**B, C**) Western blot analysis to confirm the reduced expression of HCN2 in the hippocampus of WT mice. (**B**), representative protein bands of HCN2; (**C**), quantification of the relative HCN2 levels in the hippocampus (EGFP, $n=6$; HCN2-shRNA, $n=5$). Unpaired t-test: $t_{(9)}=4.842$, $p=0.0009$. ***$p<0.001$. (**D**) Representative traces elicited by a series of negative current injections in the dCA1 PNs of WT mice with (brown) or without (black) knocking down the expression of HCN2. (**E**) The sag ratios detected in the dCA1 PNs of WT mice with or without knocking down the expression of HCN2, $n=10$ (EGFP) or 8 (HCN2-shRNA). Unpaired t-test: $t_{(16)}=5.086$, $p=0.0001$. ***$p<0.001$. (**F**) Sag amplitudes of dCA1 PNs in WT mice with or without knocking down the expression of HCN2 at −200 to 0-pA current injections. Two-way ANOVA: virus (HCN2-shRNA), $F_{(1, 16)}=13.86$, $p=0.0018$; current step, $F_{(1.994, 31.90)}=330.7$, $p<0.0001$; interaction, $F_{(4, 64)}=3.772$, $p=0.0081$; *$p<0.05$, **$p<0.01$ with Bonferroni's post-hoc test. (**G**) Representative traces of the HCN-conducted I_h currents in dCA1 PNs of WT mice with or without knocking down the expression of HCN2. (**H**) Quantification of the I_h currents (EGFP, $n=8$ cells from 5 mice; HCN2-shRNA, $n=8$ cells from 5 mice). Two-way ANOVA: virus (HCN2-shRNA), $F_{(1, 14)}=27.95$, $p=0.0001$; voltage step, $F_{(1.281, 17.94)}=533.1$, $p<0.0001$; interaction, $F_{(6, 84)}=26.51$, $p<0.0001$; **$p<0.01$, ***$p<0.001$ with Bonferroni's post-hoc test. (**I**) Representative traces of sAP of dCA1 PNs in WT mice with or without knocking down the expression of HCN2. (**J**) Quantification of the sAP frequencies in the dCA1 PNs of WT mice with or without knocking down HCN2 (EGFP, $n=27$ cells from 10 mice; HCN2-shRNA, $n=28$ cells from 10 mice). Unpaired t-test: $t_{(53)}=2.081$, $p=0.0423$. *$p<0.05$. (**K**) Representative traces showing LTP in CA1 of WT mice with or without knocking down the expression of HCN2. (**L**) Quantification of the last 15 min of the fEPSP recordings (EGFP, $n=9$ cells from 5 mice; HCN2-shRNA, $n=8$ cells from 5 mice). Unpaired t-test: $t_{(15)}=1.757$, $p=0.0993$. **(M)** The percentage of the alternations in Y-maze tests of WT mice with or without knocking down the expression of HCN2 (WT/EGFP: $n=10$; WT/HCN2-shRNA: $n=11$). Unpaired t-test: $t_{(19)}=4.659$, $p=0.0002$. ***$p<0.001$. **(N)** The discrimination index of novel location recognition (NLR) test of WT mice with or without knocking down the expression of HCN2 (WT/EGFP: $n=10$; WT/HCN2-shRNA: $n=11$). Unpaired t-test: $t_{(19)}=3.588$, $p=0.0020$. **$p<0.01$

of HCN2, we injected AAV-mCaMK2α-eGFP-shRNAmir (mHCN2) into the CA1 to knock down the expression of HCN2 in CA1 PNs of WT mice. As shown in Fig. 8A, the virus was dominantly expressed in the CA1 field. Results of western blot confirmed that the expression of HCN2 was significantly reduced in the hippocampus of WT mice after injection of the virus (Fig. 8B, C). We then performed whole cell recordings in acute brain slices to examine the HCN function and the excitability of CA1 PNs. Our results revealed that reducing the expression of HCN2 significantly decreased the sag ratio and amplitude (Fig. 8D-F) and the I_h currents (Fig. 8G-H), and increased the frequency of sAPs in dCA1 PNs (Fig. 8I-J), suggesting that the HCN function was impaired and the excitability was increased in dCA1 PNs of WT mice after knocking down HCN2. These results are similar to the findings in dCA1 PNs of hAPP-J20 mice (Fig. 7). Behavioral tests of Y maze and novel location recognition showed that

reducing HCN2 in CA1 impaired the memory of WT mice (Fig. 8M, N). The CA1 LTP at the Schaffer collateral inputs, however, was slightly but not significantly decreased in CA1 of WT mice after knocking down the expression of HCN2 (Fig. 8K, L).

Overexpressing HCN2 in dCA1 did not affect the deposition of Aβ and inflammation in the hippocampus of hAPP-J20 mice

To evaluate the effects of modulating HCN2 expression on the amyloid pathology and inflammation in hAPP-J20 mice, we did immunostaining to assess the Aβ deposition and glial cells ($GFAP^+$ and $Iba1^+$) in the hippocampus of hAPP-J20 mice after overexpression of HCN2 in the hippocampal pyramidal neurons. The numbers of both $GFAP^+$ and $Iba1^+$ cells were increased in the hippocampus of hAPP-J20 mice versus WT mice (Fig. S8C-F). However, they were not affected in the hippocampus of both WT and hAPP-J20 mice after HCN2 overexpression (Fig. S8C-F). Overexpressing HCN2 in dCA1 for two weeks did not affect the Aβ plaque load in the hippocampus of hAPP-J20 mice (Fig. S8A, B). Together, our data suggested that increasing HCN2 expression in the dCA1 pyramidal neurons did not affect the amyloid pathology or inflammation in hAPP-J20 mice.

Discussion

Hyperactivity of CA1 PNs is one of the early events in AD [7]. Aβ-induced suppression of glutamate reuptake may partially explain why CA1 PNs are hyperactive [16]. On the other hand, reduced inhibitory synaptic transmission was reported to contribute to the hyperactivity of CA1 PNs in 2.5-month-old 5×FAD mice [14]. However, Hijazi et al. reported that PV neurons were hyperactive and spontaneous inhibitory inputs onto hippocampal CA1 PNs were increased in APP/PS1 mice at the age of around 4-month-old [52]. Clearly, more studies are needed to further investigate the role of inhibitory transmission in the early hyperactivity of CA1 PNs in AD. Recent studies of both rat and mouse models of AD suggest that the abnormal intrinsic membrane properties play a major role in the hyperactivity of CA1 PNs [18, 42]. However, the mechanisms underlying the abnormal intrinsic membrane properties of CA1 PNs in AD remain elusive.

In the present study, our data show that the Aβ-induced dysregulation of HCNs is associated with the hyperexcitability of dCA1 PNs in AD mice, which is inline with previous literatures [31, 34]. HCN channelopathy was also reported in the hippocampus of mice expressing a human tauopathy-associated tau fragment [33]. Therefore, both Aβ and tau, the two hallmarks of AD, could affect HCNs, suggesting that HCNs may indeed be involved in the pathogenesis of AD. We further provide evidence showing that the expression of HCN2 is reduced in CA1 neurons of AD mice and AD patients, and specifically overexpressing HCN2 attenuates the hyperexcitability of dCA1 PNs in AD mice, suggesting that deficiency of HCN2 is associated with the hyperexcitability of dCA1 PNs in AD mice. Knocking down the expression of HCN2 increased the excitability of dCA1 PNs in WT mice, further indicating the association between deficiency of HCN2 and hyperexcitability of CA1 PNs. Our data, however, did not exclude the possibility that HCN1 or the alteration of the relative levels of HCN1 and HCN2 is also involved in the hyperexcitability of CA1 PNs in AD. Targeting dCA1 PNs may also lead to compensatory changes in vCA1 PNs and therefore affects the circuit activity in the hippocampus. It will be interesting to examine the excitability of vCA1 PNs after overexpressing or knocking down HCN2 in dCA1 PNs in future studies. In addition, the hyperexcitability of dCA1 PNs in hAPP-J20 mice likely arises from a combination of different factors. While our data show the association between HCN2 deficiency and neuronal excitability, we acknowledge that other factors such as the morphological changes (for instance, dendritic degeneration of CA1 PNs) [41, 42] are important contributors as well.

One of the major effects of HCN channels is altering the RMP of neurons [20]. However, although the expression of HCN2 was reduced and the activity of HCN channels was impaired, we did not observe a difference in the RMP of dCA1 PNs between WT and hAPP-J20 mice. Similar to our results, Rizzello et al. reported in Tg2576 mice that CA1 PNs are hyperexcitable and the HCN channels underlying the Ih current are less active in CA1 PNs, however, the RMP of CA1 PNs is similar between Tg2576 and WT mice [31]. We believe that some compensatory changes contribute to the unaltered RMP of CA1 PNs in APP mice under the circumstance of HCN deficiency, and more studies are needed to further investigate this possibility.

Treatment with lamotrigine restored the activity of HCN channels, reduced the excitability of CA1 PNs and improved memory in Tg2576 mice [31], suggesting that the hyperexcitability of CA1 PNs mediated by HCN channelopathy may be associated with the memory deficits of AD mice. However, due to the fact that lamotrigine is nonspecific for HCNs and nonselective among subtypes of HCN channels, it is not clear whether the HCN channelopathy is indeed the reason for hyperexcitability of CA1 PNs or memory deficits of AD mice. It is not clear either which subtype(s) of HCNs account for the hyperexcitability of CA1 PNs in AD. We found that the expression of HCN2 was reduced in CA1 neurons of AD patients and AD mice, and overexpressing HCN2 not only reduced the hyperexcitability of dCA1 PNs but also improved cognitive functions of hAPP-J20 mice. Furthermore, reducing the expression of HCN2 enhanced the

excitability of dCA1 PNs and impaired the memory in WT mice. These results suggest that the hyperexcitability of dCA1 PNs which is associated with the dysregulation of HCN2 contributes to the memory deficits in AD mice. The fact that direct inhibition of dCA1 PNs improved cognitive functions in hAPP-J20 mice further supports the connection between the hyperexcitability of dCA1 PNs and the memory deficits in AD.

Although overexpressing HCN2 improves memory in hAPP-J20 mice, it impairs memory in WT mice. The differential behavioral outcomes of HCN2 overexpression may underscore the context-dependent nature of HCN2 function. In J20 mice, where baseline HCN2 expression and function are reduced, overexpression restores HCN2 to more normal levels, improving cognitive performance. In contrast, WT mice exhibit normal HCN2 expression under baseline conditions, and overexpression likely results in supraphysiological levels of HCN2 activity. This disruption of the excitability balance may impair network homeostasis, leading to cognitive deficits. These findings emphasize the importance of maintaining optimal HCN2 levels for normal cognitive function and suggest that therapeutic interventions should aim to restore, rather than excessively enhance, HCN2 activity. In addition, the effects of HCN2 overexpression on the input resistance of CA1 PNs in hAPP-J20 mice may be mediated by direct increase of HCNs and indirect outcomes such as morphological changes of neurons or other compensatory mechanisms.

Hijazi et al. reported that PV neurons were hyperexcitable and the spontaneous inhibitory transmission onto CA1 PNs was increased in young APP/PS1 mice [52]. However, we found in a previous study that both spontaneous inhibitory and spontaneous excitatory transmissions onto the CA1 PNs were comparable between hAPP-J20 and WT mice at the age of 4–5 months [42], which is similar to the results of studies in a rat model of AD [18]. In another study, Li et al. reported that inhibitory transmission onto the CA1 PNs was reduced in the early stage of 5×FAD mice [14]. In addition, our results in the present study showed that the excitability of PV neurons in the CA1 area of 6-month-old hAPP-J20 mice was not different from that of WT mice. Apparently, data regarding the excitability of GABAergic neurons and the synaptic transmission onto CA1 PNs of AD mice are inconsistent, and the discrepancies could be caused by the different lines of AD models, different ages of mice or different approaches used in those different research groups. Nevertheless, more studies are warranted to clarify those discrepancies.

While there are studies reporting that modulating HCN channels affected the Aβ levels [27, 53], we did not observe a difference in the deposition of Aβ in the hippocampus of hAPP-J20 mice with or without overexpressing HCN2 in dCA1 PNs. Previous studies reported that chronic activation of perforant pathway enhanced the Aβ pathology in APP transgenic mice [54]. We therefore expected that inhibiting hippocampal pyramidal neurons may reduce the Aβ deposition. However, we found that chemogenetic inhibition of dCA1 PNs for two weeks did not significantly affect the Aβ plaques in the hippocampus of hAPP-J20 mice. Although our data did not exclude the possibility that overexpressing HCN2 or inhibiting dCA1 PNs for a longer period of time may reduce the Aβ levels, it indeed suggested that reducing Aβ was not absolutely required to improve cognitive functions of AD mice.

Limitations of this study: Our findings demonstrate a correlation between HCN2 deficiency, hyperexcitability of dCA1 pyramidal neurons, and memory deficits in hAPP-J20 mice. While our data suggest that HCN2 plays a role in regulating neuronal excitability, further studies are needed to establish a causal relationship and to dissect the contributions of other factors, such as morphological changes and additional ion channels. Second, the behavioral outcomes of HCN2 overexpression highlight the importance of maintaining a physiological balance of HCN2 activity. While our results suggest that HCN2 overexpression restores normal function in J20 mice, the cognitive impairments observed in WT mice following overexpression suggest that supraphysiological levels of HCN2 disrupt network homeostasis. Future studies should explore the dose-dependent effects of HCN2 modulation to better understand the therapeutic window for interventions targeting HCN2. Finally, the non-selective nature of cAMP (as an HCN activator) and ZD-7288 (as an HCN blocker) limits our ability to attribute the observed effects specifically to HCN2. While prior evidence and our data suggest a role for HCN2, further experiments using more selective tools, such as HCN2-specific modulators or genetic approaches, are needed to confirm our conclusions.

Conclusions

In summary, we show here that dysregulation of HCN channels, particularly HCN2, is associated with the hyperexcitability of dCA1 PNs in hAPP-J20 mice likely by regulating the intrinsic membrane properties. Furthermore, overexpressing HCN2 in dCA1 PNs improves cognitive performance of hAPP-J20 mice without affecting the Aβ pathology and inflammation in the hippocampus. Our findings thus open the possibility that modulating HCN channels, especially HCN2, could be a new approach to prevent the aberrant activity of dCA1 PNs and then improve cognitive functions in AD. Unfortunately, specific modulators for subtypes of HCNs are lacking. But a new progress of developing selective and brain-penetrant HCN1 inhibitors [55] may facilitate the

identification of new specific modulators for HCNs and therefore provide new strategies for treating AD.

Abbreviations

AD	Alzheimer's Disease
Aβ	Amyloidβ
hAPP	human Amyloid Precursor Protein
WT	Wild Type
PNs	Pyramidal Neurons
dCA1	dorsal CA1
vCA1	ventral CA1
DG	Dentate Gyrus
PV	Parvalbumin
CNO	Clozapine N-oxide
aCSF	artificial Cerebrospinal Fluid
fEPSPs	field Excitatory Postsynaptic Potentials
IOD	Integrated Optical Density
SLM	Stratum Lacunosum-Molecularis
SR	Stratum Radiatum
OR	Stratum Oreins
NLR	Novel Location Recognition
RMP	Resting Membrane Potential
LTP	Long Term Potentiation
sAPs	spontaneous Action Potentials
DREADDs	Designer Receptors Exclusively Activated by Designer Drugs

Supplementary Information

The online version contains supplementary material available at https://doi.org/10.1186/s13195-025-01704-y.

Supplementary Material 1

Acknowledgements

We thank Janssen Research & Development, L.L.C. for providing 3D6, the National Human Brain Bank for Health and Disease at Zhejiang University for providing human brain sections, and Dr. Sanhua Fang, Li Liu from the Core Facilities of Zhejiang University School of Medicine for technical support. We also thank Dr. Liping Li of Ningbo University for providing Aβ oligomers.

Author contributions

X.Q.Z. and B.S. designed the experiments; X.Q.Z. and T.Z. did the electrophysiological experiments; T.Z., Y.P.Z., J.W. and C.L. did the ELISA and immunostaining; T.Z. and X.J.W. did the western blots; T.Z., Y.P.Z. and H.Q.Z. did the virus injection, chemogenetics, and behavioral tests with assistance from C.L. and Q.S.; X.Q.Z., Y.P.Z. and H.W.S. performed the data analysis; B.S. and X.Q.Z. wrote the manuscript with inputs from other authors.

Funding

This work was supported by the National Natural Science Foundation of China (32201322, 32271028, 32071031, 32471030), the National Key R&D Program of China (2021YFA1101701, 2019YFA0110103) and the Natural Science Foundation of Zhejiang Province (LY24H090001, LZ25C090001).

Data availability

No datasets were generated or analysed during the current study.

Declarations

Ethics approval and consent to participate

Not applicable.

Consent for publication

Not applicable.

Competing interests

The authors declare no competing interests.

Author details

[1]Department of Pharmacology, Health Science Center of Ningbo University, Ningbo, Zhejiang Province 315211, China
[2]Department of Anesthesiology of the Children's Hospital and School of Brain Science and Brain Medicine, Zhejiang University School of Medicine and National Clinical Research Center for Child Health; NHC and CAMS Key Laboratory of Medical Neurobiology, School of Brain Science and Brain Medicine, Zhejiang University, Hangzhou, Zhejiang Province 310058, China
[3]Department of Neurology, The First Affiliated Hospital of Ningbo University, 59 Liuting Street, Haishu District, Ningbo, Zhejiang Province 315211, China
[4]Zhejiang Pharmaceutical College, Ningbo, Zhejiang Province 315100, China

Received: 18 September 2024 / Accepted: 19 February 2025
Published online: 27 February 2025

References

1. Busche MA, Hyman BT. Synergy between amyloid-β and Tau in Alzheimer's disease. Nat Neurosci. 2020;23(10):1183–93. https://doi.org/10.1038/s41593-020-0687-6.
2. Knopman DS, Amieva H, Petersen RC, et al. Alzheimer disease. Nat Rev Dis Primers. 2021;7(1):33. https://doi.org/10.1038/s41572-021-00269-y.
3. Selkoe DJ, Hardy J. The amyloid hypothesis of Alzheimer's disease at 25 years. EMBO Mol Med. 2016;8(6):595–608. https://doi.org/10.15252/emmm.201606210.
4. Selkoe DJ. The advent of alzheimer treatments will change the trajectory of human aging. Nat Aging. 2024;4(4):453–63. https://doi.org/10.1038/s43587-024-00611-5.
5. Busche MA, Chen X, Henning HA, et al. Critical role of soluble amyloid-β for early hippocampal hyperactivity in a mouse model of Alzheimer's disease. Proc Natl Acad Sci USA. 2012;109(22):8740–5. https://doi.org/10.1073/pnas.1206171109.
6. Busche MA, Eichhoff G, Adelsberger H, et al. Clusters of hyperactive neurons near amyloid plaques in a mouse model of Alzheimer's disease. Science. 2008;321(5896):1686–9. https://doi.org/10.1126/science.1162844.
7. Busche MA, Konnerth A. Impairments of neural circuit function in Alzheimer's disease. Philos Trans R Soc Lond B Biol Sci. 2016;371(1700):20150429. https://doi.org/10.1098/rstb.2015.0429.
8. Busche MA, Wegmann S, Dujardin S, et al. Tau impairs neural circuits, dominating amyloid-β effects, in alzheimer models in vivo. Nat Neurosc. 2019;22(1):57–64. https://doi.org/10.1038/s41593-018-0289-8.
9. Marinković P, Blumenstock S, Goltstein PM, et al. In vivo imaging reveals reduced activity of neuronal circuits in a mouse tauopathy model. Brain. 2019;142(4):1051–62. https://doi.org/10.1093/brain/awz035.
10. Palop JJ, Chin J, Roberson ED, et al. Aberrant excitatory neuronal activity and compensatory remodeling of inhibitory hippocampal circuits in mouse models of Alzheimer's disease. Neuron. 2007;55(5):697–711. https://doi.org/10.1016/j.neuron.2007.07.025.
11. Palop JJ, Mucke L. Network abnormalities and interneuron dysfunction in alzheimer disease. Nat Rev Neurosci. 2016;17(12):777–92. https://doi.org/10.1038/nrn.2016.141.
12. Cai W, Li L, Sang S, Pan X, Zhong C. Physiological roles of β-amyloid in regulating synaptic function: implications for AD pathophysiology. Neurosci Bull. 2023;39(8):1289–308. https://doi.org/10.1007/s12264-022-00985-9.
13. Counts SE, Alldred MJ, Che S, Ginsberg SD, Mufson EJ. Synaptic gene dysregulation within hippocampal CA1 pyramidal neurons in mild cognitive impairment. Neuropharmacology. 2014;79:172–9. https://doi.org/10.1016/j.neuropharm.2013.10.018.
14. Li Y, Zhu K, Li N, et al. Reversible GABAergic dysfunction involved in hippocampal hyperactivity predicts early-stage alzheimer disease in a mouse model. Alzheimers Res Ther. 2021;13(1):114. https://doi.org/10.1186/s13195-021-00859-8.
15. Roberson ED, Scearce-Levie K, Palop JJ, et al. Reducing endogenous Tau ameliorates amyloid beta-induced deficits in an Alzheimer's disease mouse model. Science. 2007;316(5825):750–4. https://doi.org/10.1126/science.1141736.

16. Zott B, Simon MM, Hong W, et al. A vicious cycle of B amyloid-dependent neuronal hyperactivation. Science. 2019;365(6453):559–65. https://doi.org/10.1126/science.aay0198.
17. Šišková Z, Justus D, Kaneko H, et al. Dendritic structural degeneration is functionally linked to cellular hyperexcitability in a mouse model of Alzheimer's disease. Neuron. 2014;84(5):1023–33. https://doi.org/10.1016/j.neuron.2014.10.024.
18. Sosulina L, Mittag M, Geis HR, et al. Hippocampal hyperactivity in a rat model of Alzheimer's disease. J Neurochem. 2021;157(6):2128–44. https://doi.org/10.1111/jnc.15323.
19. Yao J, Sun B, Institoris A, et al. Limiting RyR2 open time prevents Alzheimer's Disease-Related neuronal hyperactivity and memory loss but not β-Amyloid accumulation. Cell Rep. 2020;32(12):108169. https://doi.org/10.1016/j.celrep.2020.108169.
20. Biel M, Wahl-Schott C, Michalakis S, Zong X. Hyperpolarization-activated cation channels: from genes to function. Physiol Rev. 2009;89(3):847–85. https://doi.org/10.1152/physrev.00029.2008.
21. Combe CL, Gasparini S. I(h) from synapses to networks: HCN channel functions and modulation in neurons. Prog Biophys Mol Biol. 2021;166:119–32. https://doi.org/10.1016/j.pbiomolbio.2021.06.002.
22. Kazmierska-Grebowska P, Jankowski MM, MacIver MB. Missing puzzle pieces in dementia research: HCN channels and Theta oscillations. Aging Dis. 2024;15(1):22–42. https://doi.org/10.14336/ad.2023.0607.
23. Notomi T, Shigemoto R. Immunohistochemical localization of ih channel subunits, HCN1-4, in the rat brain. J Com Neurol. 2004;471(3):241–76. https://doi.org/10.1002/cne.11039.
24. Moosmang S, Biel M, Hofmann F, Ludwig A. Differential distribution of four hyperpolarization-activated cation channels in mouse brain. Biol Chem. 1999;380(7–8):975–80. https://doi.org/10.1515/bc.1999.121.
25. Bender RA, Soleymani SV, Brewster AL, et al. Enhanced expression of a specific hyperpolarization-activated Cyclic nucleotide-gated cation channel (HCN) in surviving dentate gyrus granule cells of human and experimental epileptic hippocampus. J Neurosci. 2003;23(17):6826–36. https://doi.org/10.1523/jneurosci.23-17-06826.2003.
26. Chang X, Wang J, Jiang H, Shi L, Xie J. Hyperpolarization-Activated Cyclic Nucleotide-Gated channels: an emerging role in neurodegenerative diseases. Front Mol Neurosci. 2019;12:141. https://doi.org/10.3389/fnmol.2019.00141.
27. Saito Y, Inoue T, Zhu G, et al. Hyperpolarization-activated Cyclic nucleotide gated channels: a potential molecular link between epileptic seizures and Aβ generation in Alzheimer's disease. Mol Neurodegener. 2012;7:50. https://doi.org/10.1186/1750-1326-7-50.
28. Musial TF, Molina-Campos E, Bean LA, et al. Store depletion-induced h-channel plasticity rescues a channelopathy linked to Alzheimer's disease. Neurobiol Learn Mem. 2018;154:141–57. https://doi.org/10.1016/j.nlm.2018.06.004.
29. Russo ML, Molina-Campos E, Ybarra N, et al. Variability in sub-threshold signaling linked to Alzheimer's disease emerges with age and amyloid plaque deposition in mouse ventral CA1 pyramidal neurons. Neurobiol Aging. 2021;106:207–22. https://doi.org/10.1016/j.neurobiolaging.2021.06.018.
30. Hall AM, Throesch BT, Buckingham SC, et al. Tau-dependent Kv4.2 depletion and dendritic hyperexcitability in a mouse model of Alzheimer's disease. J Neurosci. 2015;35(15):6221–30. https://doi.org/10.1523/jneurosci.2552-14.2015.
31. Rizzello E, Pimpinella D, Pignataro A, et al. Lamotrigine rescues neuronal alterations and prevents seizure-induced memory decline in an Alzheimer's disease mouse model. Neurobiol Dis. 2023;181:106106. https://doi.org/10.1016/j.nbd.2023.106106.
32. Haytural H, Benfeitas R, Schedin-Weiss S, et al. Insights into The changes in The proteome of alzheimer disease elucidated by a meta-analysis. The proteome of alzheimer disease elucidated by a meta-analysis. Sci Data. 2021;8(1):312. https://doi.org/10.1038/s41597-021-01090-8.
33. Goniotaki D, Tamagnini F, Biasetti L, et al. Tau-mediated synaptic dysfunction is coupled with HCN channelopathy. Alzheimers Dement. 2024;20(8):5629–46. https://doi.org/10.1002/alz.14074.
34. Eslamizade MJ, Saffarzadeh F, Mousavi SM, et al. Alterations in CA1 pyramidal neuronal intrinsic excitability mediated by ih channel currents in a rat model of amyloid beta pathology. Neuroscience. 2015;305:279–92. https://doi.org/10.1016/j.neuroscience.2015.07.087.
35. Fu XX, Duan R, Wang SY, et al. Lamotrigine protects against cognitive deficits, synapse and nerve cell damage, and hallmark neuropathologies in a mouse model of Alzheimer's disease. Neural Regen Res. 2023;18(1):189–93. https://doi.org/10.4103/1673-5374.343888.
36. Mucke L, Masliah E, Yu GQ, et al. High-level neuronal expression of Abeta 1–42 in wild-type human amyloid protein precursor Transgenic mice: synaptotoxicity without plaque formation. J Neurosci. 2000;20(11):4050–8. https://doi.org/10.1523/jneurosci.20-11-04050.2000.
37. Mou CY, Xie YF, Wei JX, et al. Rose Bengal inhibits β-amyloid oligomers-induced Tau hyperphosphorylation via acting on Akt and CDK5 kinases. Psychopharmacology. 2022;239(11):3579–93. https://doi.org/10.1007/s00213-022-06232-3.
38. Zhang X, Mei Y, He Y, et al. Ablating adult neural stem cells improves synaptic and cognitive functions in alzheimer models. Stem Cell Rep. 2021;16(1):89–105. https://doi.org/10.1016/j.stemcr.2020.12.003.
39. Zhang XQ, Xu L, Yang SY, et al. Reduced synaptic transmission and intrinsic excitability of a subtype of pyramidal neurons in the medial prefrontal cortex in a mouse model of Alzheimer's disease. J Alzheimers Dis. 2021;84(1):129–40. https://doi.org/10.3233/jad-210585.
40. Chu HY, Gu Q, Jin GZ, Hu GY, Zhen X. Electrophysiological effects of SKF83959 on hippocampal CA1 pyramidal neurons: potential mechanisms for the drug's neuroprotective effects. PLoS ONE. 2010;5(10):e13118. https://doi.org/10.1371/journal.pone.0013118.
41. Sun B, Zhou Y, Halabisky B, et al. Cystatin C-cathepsin B axis regulates amyloid beta levels and associated neuronal deficits in an animal model of Alzheimer's disease. Neuron. 2008;60(2):247–57. https://doi.org/10.1016/j.neuron.2008.10.001.
42. Wang J, Mei Y, Zhang X, et al. Aberrant serotonergic signaling contributes to the hyperexcitability of CA1 pyramidal neurons in a mouse model of Alzheimer's disease. Cell Rep. 2023;42(3):112152. https://doi.org/10.1016/j.celrep.2023.112152.
43. Zhang X, Wei X, Mei Y, et al. Modulating adult neurogenesis affects synaptic plasticity and cognitive functions in mouse models of Alzheimer's disease. Stem Cell Rep. 2021;16(12):3005–19. https://doi.org/10.1016/j.stemcr.2021.11.003.
44. Cheng IH, Scearce-Levie K, Legleiter J, et al. Accelerating amyloid-beta fibrillization reduces oligomer levels and functional deficits in alzheimer disease mouse models. J Biol Chem. 2007;282(33):23818–28. https://doi.org/10.1074/jbc.M701078200.
45. Chin J, Palop JJ, Puoliväli J, et al. Fyn Kina J Neurosci. 2005;25(42):9694–703. https://doi.org/10.1523/jneurosci.2980-05.2005.
46. Ognibene E, Middei S, Daniele S, et al. Aspects of Spatial memory and behavioral disinhibition in Tg2576 Transgenic mice as a model of Alzheimer's disease. Behav Brain Res. 2005;156(2):225–32. https://doi.org/10.1016/j.bbr.2004.05.028.
47. Roth BL. DREADDs for neuroscientists. Neuron. 2016;89(4):683–94. https://doi.org/10.1016/j.neuron.2016.01.040.
48. Hammelmann V, Stieglitz MS, Hülle H, et al. Abolishing cAMP sensitivity in HCN2 pacemaker channels induces generalized seizures. JCI Insight. 2019;4(9):e126418. https://doi.org/10.1172/jci.insight.126418.
49. Lee CH, MacKinnon R. Structures of the human HCN1 Hyperpolarization-Activated channel. Cell. 2017;168(1–2):111–e12011. https://doi.org/10.1016/j.cell.2016.12.023.
50. Xie Y, Zheng J, Li S, et al. GLP-1 improves the neuronal supportive ability of astrocytes in Alzheimer's disease by regulating mitochondrial dysfunction via the cAMP/PKA pathway. Biochem Pharmacol. 2021;188:114578. https://doi.org/10.1016/j.bcp.2021.114578.
51. Harris NC, Constanti A. Mechanism of block by ZD 7288 of the hyperpolarization-activated inward rectifying current in guinea pig substantia Nigra neurons in vitro. J Neurophysiol. 1995;74(6):2366–78. https://doi.org/10.1152/jn.1995.74.6.2366.
52. Hijazi S, Heistek TS, Scheltens P, et al. Early restoration of parvalbumin interneuron activity prevents memory loss and network hyperexcitability in a mouse model of Alzheimer's disease. Mol Psychiatry. 2020;25(12):3380–98. https://doi.org/10.1038/s41380-019-0483-4.
53. Frykman S, Inoue M, Ikeda A, et al. Maturation and processing of the amyloid precursor protein is regulated by the potassium/sodium hyperpolarization-activated Cyclic nucleotide-gated ion channel 2 (HCN2). Biochem Biophysl Res Commun. 2017;483(1):352–8. https://doi.org/10.1016/j.bbrc.2016.12.140.
54. Yamamoto K, Tanei ZI, Hashimoto T, et al. Chronic optogenetic activation augments Aβ pathology in a mouse model of alzheimer disease. Cell Rep. 2015;11(6):859–65. https://doi.org/10.1016/j.celrep.2015.04.017.

55. Harde E, Hierl M, Weber M, et al. Selective and brain-penetrant HCN1 inhibitors reveal links between synaptic integration, cortical function, and working memory. Cell Chem Biol. 2024;31(3):577–e59223. https://doi.org/10.1016/j.chembiol.2023.11.004.

Publisher's note